Internal states of model isotropic granular packings. I. Assembling process, geometry and contact networks.

Ivana Agnolin, Jean-Noël Roux

Internal states of model isotropic granular packings. I. Assembling process, geometry and contact networks.

Ivana Agnolin and Jean-Noël Roux*
Laboratoire des Matériaux et des Structures du Génie Civil†*, Institut Navier, 2 allée Kepler, Cité Descartes, 77420 Champs-sur-Marne, France*
(Dated: May 22, 2007)

This is the first paper of a series of three, reporting on numerical simulation studies of geometric and mechanical properties of static assemblies of spherical beads under an isotropic pressure. The influence of various assembling processes on packing microstructures are first investigated. Properties of frictionless and frictional packings are discussed and compared. Frictionless systems assemble in the unique random close packing state in the low pressure limit if the compression process is fast enough, and higher solid fractions correspond to more ordered configurations with traces of crystallization. Specific properties directly related to isostaticity of the force-carrying structure in the rigid limit are discussed – in particular a simple relationship between the force distribution and the pressure-dependent bulk modulus under isotropic stresses. With frictional grains, different preparation procedures result in quite different inner structures that cannot be classified by the sole density. While "lubricated" systems, in which friction mobilization is suppressed or strongly reduced in the assembling stage, achieve random close packing densities with high coordination number $z^* = 6$ in the rigid limit (z^* counting the average number of contacts per force-carrying grain), an idealized "vibration" procedure, in which the grains are maintained in an agitated, collisional régime up to high densities, is shown to result, for the same solid fractions, in much lower coordination numbers: $z^* \simeq 4.5$ at low pressures. Different microstructures are characterized in terms of near neighbor correlations on various scales, and some comparisons with available laboratory data are reported, although values of contact coordination numbers apparently remain experimentally inaccessible. Low coordination packings have a large proportion (>10%) of rattlers – grains carrying no force – the effect of which should be accounted for on studying position correlations, and might also contain a small proportion of harmless "floppy modes" associated with divalent grains. Low pressure states of frictional packings retain a finite level of force indeterminacy even when assembled with the slowest compression rates simulated, except in the case when the friction coefficient tends to infinity.

PACS numbers: 45.70.-n, 83.80.Fg, 46.65.+g, 62.20.Fe

I. INTRODUCTION

A. Context and motivations

The mechanical properties of solidlike granular packings and their microscopic, grain-level origins are an active field of research in material science and condensed-matter physics [1, 2, 3]. Motivations are practical, originated in soil mechanics and material processing, as well as theoretical, as general approaches to the rheology of different physical systems made of particle assemblies out of thermal equilibrium [4] are attempted.

The packing of equal-sized spherical balls is a simple model for which there is a long tradition of *geometric* characterization studies. Packings are usually classified according to their density or solid volume fraction Φ, and the frequency of occurrence of some local patterns. Direct observations of packing microstructure is difficult, although it has recently benefitted from powerful imaging techniques [5, 6, 7]. The concept of random close packing (RCP), is often invoked [8, 9], although some authors criticized it as ill-defined [10]. It corresponds to the common observation that bead packings without any trace of crystalline order do not exceed a maximum density, Φ_{RCP}, slightly below 0.64 [8].

Mechanical studies in the laboratory have been performed on granular materials for decades in the realm of soil mechanics, and the importance of packing fraction Φ on the rheological behavior has long been recognized [1, 11, 12, 13]. The anisotropy of the packing microstructure, due to the assembling process, has also been investigated [14, 15], and shown to influence the stress-strain behavior of test samples [16], as well as the stress field and the response to perturbations of gravity-stabilized sandpiles or granular layers [17].

Discrete numerical simulation [18] proved a valuable tool to investigate the internal state of packings, as it is able to reproduce mechanical behaviors, and to identify relevant variables other than Φ, such as coordination number and fabric (or distribution of contact orientations) [19, 20, 21, 22, 23]. In the case of sphere packings, simulations have been used to characterize the geometry of gravity-deposited systems [24, 25] or oedometrically

†LMSGC is a joint laboratory depending on Laboratoire Central des Ponts et Chaussées, École Nationale des Ponts et Chaussées and Centre National de la Recherche Scientifique
*Electronic address: jean-noel.roux@lcpc.fr

compressed ones [26], to investigate the quasistatic, hysteretic stress-strain dependence in solid packings [27, 28], and their pressure-dependent elastic moduli in a compression experiment [29, 30].

However, in spite of recent progress, quite a few basic questions remain unresolved. It is not obvious how closely dense samples used in numerical simulations actually resemble laboratory ones, for which density is often the only available state parameter. Both simulations and experiments resort to certain preparation procedures to assemble granular packings, which, although their influence is recognized as important, are seldom studied, or even specified. One method to produce dense packings in simulations is to set the coefficient of intergranular friction to zero [26, 27] or to a low value [28] in the assembling stage, while a granular gas gets compacted and equilibrated under pressure. On keeping frictionless contacts, this results, in the limit of low confining stress, in dense systems with rather specific properties [30, 31], related to isostaticity and potential energy minimization [32]. Examples of traditional procedures in soil mechanics are rain deposition under gravity, also known as air pluviation (which produces homogeneous states if grain flow rate and height of free fall [33] are maintained constant) and layerwise deposition and dry or moist tamping. Those two methods were observed to produce, in the case of loose sands, different structures for the same packing density [34]. Densely packed particle assemblies can also be obtained in the laboratory by vibration, or application of repeated "taps" [35, 36] to a loose deposit. How close are dense experimental sphere packings to model configurations obtained on simulating frictionless particles ? How do micromechanical parameters influence the packing structure ? Is the low pressure limit singular in laboratory grain packings and in what sense ?

B. Outline of the present study

The present paper provides some answers to such questions, from numerical simulations in the simple case of isotropically assembled and compressed homogeneous packings of spherical particles. It is the first one of a series of three, and deals with the geometric characterization of low pressure isotropic states assembled by different procedures, both without and with intergranular friction. The other two, hereafter referred to as papers II [37] and III [38], respectively investigate the effects of compressions and pressure cycles, and the elastic response of the different numerical packings, with comparisons to experimental results. Although mechanical aspects are hardly dealt with in the present paper, we insist that geometry and mechanics are strongly and mutually related. We focus here on the variability of the coordination numbers, which will prove important for mechanical response properties of granular packings, and show that equilibrated packs of identical beads can have a relatively large numbers of "rattler" grains, which do not participate in force transmission. We investigate the dependence of initial states on the assembling procedure, both with and without friction. We study the effects of procedures designed to produce dense states (close to RCP), and we characterize the geometry of such states on different scales.

It should be emphasized that we do not claim here to mimic experimental assembling procedures very closely. Rather, we investigate the results of several preparation methods, which are computationnally convenient, maintain isotropy, and produce equilibrated samples with rather different characteristics. Those methods nevertheless share some important features with laboratory procedures, and we shall argue that the resulting states are plausible models for experimental samples.

The numerical model and the simulation procedures (geometric and mechanical parameters, contact law, boundary conditions) are presented in Section II, where some basic definitions and mechanical properties pertaining to granular packs are also presented or recalled. Part III discusses the properties of frictionless packings, and introduces several characterization approaches used in the general case as well. Section IV then describes different assembling procedures of frictional packings and the resulting microstructures. Section V is a conclusion.

II. MODEL, NUMERICAL PROCEDURES, BASIC DEFINITIONS

A. Intergranular forces

We consider spherical beads of diameter a (the value of which, as we ignore gravity, will prove irrelevant), interacting in their contacts by the Hertz law, relating the normal force N to the elastic normal deflection h as :

$$N = \frac{\tilde{E}\sqrt{a}}{3} h^{3/2}. \tag{1}$$

In Eqn. 1, we introduced the notation

$$\tilde{E} = \frac{E}{1-\nu^2},$$

E is the Young modulus of the beads, and ν the Poisson ratio. For spheres, h is simply the distance of approach of the centers beyond the first contact. The normal stiffness K_N of the contact is defined as the rate of change of the force with normal displacement:

$$K_N = \frac{dN}{dh} = \frac{\tilde{E}\sqrt{a}}{2} h^{1/2} = \frac{3^{1/3}}{2} \tilde{E}^{2/3} a^{1/3} N^{1/3} \tag{2}$$

In order to model tangential elasticity and friction, we resort to a simplification of the Cattaneo-Mindlin-Deresiewicz results [39] : the tangential stiffness K_T relating, in the elastic regime, the increment of tangential

reaction $d\mathbf{T}$ to the relative tangential displacement increment $d\mathbf{u}_T$ is a function of N (*i.e.,* it is kept constant, equal to its value for $\mathbf{T}=0$):

$$d\mathbf{T} = \frac{2-2\nu}{2-\nu} K_N d\mathbf{u}_T \tag{3}$$

To enforce the Coulomb condition with friction coefficient μ, $\mathbf{T}$ has to be projected back onto the circle of radius μN in the tangential plane whenever the increment given by eqn. 3 would cause its magnitude to exceed this limit. Moreover, when N decreases to $N-\delta N$, $\mathbf{T}$ is scaled down to the value it would have had if N had constantly been equal to $N-\delta N$ in the past. It is not scaled up when N increases. Such a procedure, suggested *e.g.*, in [40], avoids spurious increases of elastic energy for certain loading histories. More details are given in Appendix A.

Finally, tangential contact forces have to follow the material motion. Their magnitudes are assumed here not to be affected by rolling (*i.e.*, rotation about a tangential axis) or pivoting (*i.e.*, rotation about the normal axis), while their direction rotates with the normal vector due to rolling, and spins around it with the average spinning rate of the two spheres (to ensure objectivity). The corresponding equations are given in Appendix B.

In addition to the contact forces specified above, we introduce viscous ones, which oppose the normal relative displacements (we use the convention that positive normal forces are repulsive):

$$N^v = \alpha(h)\dot{h} \tag{4}$$

The damping coefficient α depends on elastic normal deflection h (or on elastic repulsive force N) and we choose its value as a fixed fraction ζ of the critical damping coefficient of the normal (linear) spring of stiffness $K_N(h)$ (as given by (2)) joining two beads of mass m:

$$\alpha(h) = \zeta\sqrt{2mK_N(h)}. \tag{5}$$

We do not introduce any tangential viscous force, and impose the Coulomb inequality to elastic force components only. Admittedly, the dissipation given by (4)-(5) has little physical justification, and is rather motivated by computational convenience. The influence of ζ on the numerical results should therefore be carefully assessed. The present study being focussed on equilibrium states and quasistatic compression, we generally use a strong dissipation, $\zeta = 0.98$.

The present numerical study was carried out with the elastic parameters $E = 70$GPa and $\nu = 0.3$, suitable for glass beads, while the friction coefficient is attributed a moderate, plausible value $\mu = 0.3$. (These choices are motivated by comparisons to experimental measurements of elastic moduli, to be carried out in paper III [38]). All our results will be stated in a form independent of bead diameter a.

B. Boundary conditions and stress control

The numerical results presented below were obtained on samples of $n = 4000$ beads, enclosed in a cubic or parallelipipedic cell with periodic boundary conditions.

It is often in our opinion more convenient to use pressure (or stress) than density (or strain) as a control parameter (a point we discuss below in Section III). We therefore use a stress-controlled procedure in our simulations, which is adapted from the Parrinello-Rahman molecular dynamics scheme [41]. The simulation cell has a rectangular parallelipipedic shape with lengths L_α parallel to coordinate axes i ($1 \le \alpha \le 3$). L_i values might vary, so that the system has $6N+3$ configurational degrees of freedom,which are the positions and orientations of the N particles and lengths L_i. $\Omega = L_1L_2L_3$ denotes the sample volume. We seek equilibrium states with set values $(\Sigma_\alpha)_{1\le\alpha\le3}$ of all three principal stresses $\sigma_{\alpha\alpha}$. We use the convention that compressive stresses are positive.

It is convenient to write position vectors $\mathbf{r}_i$, defining a square 3×3 matrix with L_α's on the diagonal, as

$$(1 \le i \le N) \quad \mathbf{r}_i = \underline{\underline{\mathbf{L}}} \cdot \mathbf{s}_i,$$

$\mathbf{s}_i$ denoting corresponding vectors in a cubic box of unit edge length. In addition to particle angular and linear velocities, which read

$$(1 \le i \le N) \quad \mathbf{v}_i = \underline{\underline{\mathbf{L}}} \cdot \dot{\mathbf{s}}_i + \underline{\underline{\dot{\mathbf{L}}}} \cdot \mathbf{s}_i,$$

one should evaluate time derivatives $\dot{L}_i$. Equations of motion are written for particles in the standard form, *i.e.,* ($F_i^{(\alpha)}$ denoting coordinate α of the total force $\mathbf{F}_i$ exerted on grain i)

$$(1 \le i \le N) \quad m_i\ddot{\mathbf{s}}_i = \underline{\underline{\mathbf{L}}}^{-1} \cdot \mathbf{F}_i, \tag{6}$$

and the usual equation for angular momentum, while $\dot{L}_\alpha$'s satisfy the following one, in which $\mathbf{r}_{ij}$ is the vector joining the centers of i to j, subject to the usual nearest image convention of periodic boundary conditions.

$$\begin{aligned} M\ddot{L}_\alpha = \frac{1}{L_\alpha}\left[L_\alpha^2 \sum_i m_i \left(\dot{s}_i^{(\alpha)}\right)^2 + \sum_{i<j} F_{ij}^{(\alpha)} r_{ij}^{(\alpha)} \right] \\ - \frac{\Omega}{L_\alpha}\Sigma_\alpha \end{aligned} \tag{7}$$

Within square brackets on the right-hand side of Eqn. 7, one recognizes the familiar formula [19, 42, 43] for $\Omega\sigma_{\alpha\alpha}$, $\underline{\underline{\sigma}}$ being the average stress in the sample:

$$\sigma_{\alpha\beta} = \frac{1}{\Omega}\left[\sum_i m_i v_i^\alpha v_i^\beta + \sum_{i<j} F_{ij}^{(\alpha)} r_{ij}^{(\alpha)} \right] \tag{8}$$

All three diagonal stress components should thus equate the prescribed values Σ_α at equilibrium. The acceleration term will cause the cell to expand in the corresponding

direction if the stress is too high, and to shrink if it is too low. Eqn. 7 involves a generalized mass M associated with the changes of shape of the simulation cell. M is set to a value of the order of the total mass of all particles in the sample. This choice was observed to result in collective degrees of freedom L_α approaching their equilibrium values under prescribed stress $\underline{\underline{\boldsymbol{\Sigma}}}$ somewhat more slowly (but not exceedingly so) than (rescaled) positions $\mathbf{s}$.

The original Parrinello-Rahman method was designed for conservative molecular systems, in such a way that the set of equations is cast in Lagrangian form. This implies in particular additional terms in (6), involving $\dot{\underline{\underline{\mathbf{L}}}}$. Such terms were observed to have a negligible influence on our calculations and were consequently omitted. Granular materials are dissipative, and energy conservation is not an issue (except for some elastic properties, see paper III [38]). Further discussion of the stress-controlled method is provided in Appendix C.

Our equations (6) and (7), with global degrees of freedom L_α slower than particle positions, lead to dynamics similar to those of a commonly used procedure in granular simulation [44]. This method consists in repeatedly changing the dimensions of the cell by very small amounts, then computing the motion of the grains for some interval of time. A "servo mechanism" can be used to impose stresses rather than strains [30]. Our approach might represent a simplification, as it avoids such a two-stage procedure. It should be kept in mind that we restricted our use of equation (7) to situations when changes in the dimensions of the simulation cell are very slow and gradual. The perturbation introduced in the motion of the grains, in comparison to the more familiar case of a fixed container, is very small.

C. Rigidity and stiffness matrices

In order to analyse the stability of equilibrium configurations – and small motions associated with the elastic response of an equilibrium grain packing, as will be dealt with in paper III – it is useful to provide appropriate definitions, introduce the suitable formalism and state the relevant properties of static contact networks. It is implied throughout this section that small displacements about an equilibrium configurations are dealt with to first order (as an infinitesimal motion, *i.e.* just like velocities), and related to small increments of applied forces, moments and stresses. The properties are stated in general form with special attention to the periodic boundary conditions with controlled diagonal stress components, as used in our numerical results. In order to allow for possible comparisons with results in two dimensions, the dimension of space is denoted as d. (For a brief discussion of the properties of rigidity and stiffness matrices in 2D periodic samples of disks, possibly with cohesion and rolling resistance, see also [45], in which the same conventions are used as those introduced here).

1. Definition of stiffness matrix

We consider a given configuration with bead center positions ($\mathbf{r}_i$, $1 \le i \le n$) and orientations (θ_i, $1 \le i \le n$), and cell dimensions (L_α, $1 \le \alpha \le d$). The grain center displacements $(\mathbf{u}_i)_{1\le i\le n}$ are conveniently written as

$$\mathbf{u}_i = \tilde{\mathbf{u}}_i - \underline{\underline{\epsilon}} \cdot \mathbf{r}_i,$$

with a set of displacements $\tilde{\mathbf{u}}_i$ satisfying periodic boundary conditions in the cell with the current dimensions, and the elements of the diagonal strain matrix $\underline{\underline{\epsilon}}$ express the relative shrinking deformation along each direction, $\epsilon_\alpha = -\Delta L_\alpha / L_\alpha$. Gathering all coordinates of particle (periodic) displacements and rotation increments, and strain parameters one defines a *displacement vector* in a space with dimension equal to the number of degrees of freedom $N_f = nd(d+1)/2 + d$,

$$\mathbf{U} = ((\tilde{\mathbf{u}}_i, \Delta\theta_i)_{1\le i\le n}, (\epsilon_\alpha)_{1\le\alpha\le d}) \,. \tag{9}$$

Let N_c denote the number of intergranular contacts. In every contacting pair i-j, we arbitrarily choose a "first" grain i and a "second" one j. The normal unit vector $\mathbf{n}_{ij}$ points from i to j (along the line joining centers for spheres). The relative displacement $\delta\mathbf{u}_{ij}$ is defined for spherical grains with radius R as

$$\delta\mathbf{u}_{ij} = \tilde{\mathbf{u}}_i + \delta\theta_i \times R\mathbf{n}_{ij} - \tilde{\mathbf{u}}_j + \delta\theta_j \times R\mathbf{n}_{ij} + \underline{\underline{\epsilon}} \cdot \mathbf{r}_{ij}, \tag{10}$$

in which $\mathbf{r}_{ij}$ is the vector pointing from the center of the first sphere i to the nearest image of the center of the second one j. The normal part $\delta\mathbf{u}_{ij}^N$ of $\delta\mathbf{u}_{ij}$ is the increment of normal deflection h_{ij} in the contact. (10) defines a $dN_c \times N_f$ matrix $\underline{\underline{\mathbf{G}}}$ which transforms $\mathbf{U}$ into the dN_c-dimensional vector of relative displacements at contacts $\delta\mathbf{u}$:

$$\delta\mathbf{u} = \underline{\underline{\mathbf{G}}} \cdot \mathbf{U} \tag{11}$$

In agreement with the literature on rigidity theory of frameworks [46] ($-\underline{\underline{\mathbf{G}}}$ is termed normalized rigidity matrix in that reference, which deals with central force networks), we call $\underline{\underline{\mathbf{G}}}$ the *rigidity matrix*.

In each contact a force $\mathbf{F}_{ij}$ is transmitted from i to j, which is split into its normal and tangential components as $\mathbf{F}_{ij} = N_{ij}\mathbf{n}_{ij} + \mathbf{T}_{ij}$. The static contact law (without viscous terms) expressed in Eqns. (1), (3), with the conditions stated in Section II A, relates the dN_c-dimensional contact force increment vector $\Delta\mathbf{f}$, formed with the values ΔN_{ij}, $\Delta\mathbf{T}_{ij}$ of the normal and tangential parts of all contact force increments, to $\delta\mathbf{u}$:

$$\Delta\mathbf{f} = \underline{\underline{\mathcal{K}}} \cdot \delta\mathbf{u}. \tag{12}$$

This defines the $(dN_c \times dN_c)$ matrix of contact stiffnesses $\underline{\underline{\mathcal{K}}}$. $\underline{\underline{\mathcal{K}}}$ is block diagonal (it does not couple different contacts). In simple cases the $d \times d$ block of $\underline{\underline{\mathcal{K}}}$ corresponding to contact i, j, $\underline{\underline{\mathcal{K}}}_{ij}$ is diagonal itself and contains stiffnesses $K_N(h_{ij})$ and (twice in $d = 3$ dimensions) $K_T(h_{ij})$

as given by (2) and (3):

$$\underline{\underline{\mathcal{K}}}^E_{ij} = \begin{bmatrix} K_N(h_{ij}) & 0 & 0 \\ 0 & K_T(h_{ij}) & 0 \\ 0 & 0 & K_T(h_{ij}). \end{bmatrix} \tag{13}$$

More complicated non-diagonal forms of $\underline{\underline{\mathcal{K}}}_{ij}$, which actually depend on the *direction* of the increments of relatives displacements in the contact, are found if friction is fully mobilized, or corresponding to those small motions reducing the normal contact force. The effects of such terms is small, with our choice of parameters, and is discussed in paper III [38].

External forces $\mathbf{F}_i$ and moments $\mathbf{\Gamma}_i$ (at the center) applied to the grains, and diagonal Cauchy stress components Σ_α can be gathered in one N_f-dimensional *load vector* $\mathbf{F}^{\text{ext}}$:

$$\mathbf{F}^{\text{ext}} = \left((\mathbf{F}_i, \mathbf{\Gamma}_i)_{1\leq i\leq n}, (\Omega\Sigma_\alpha)_{1\leq\alpha\leq d}\right), \tag{14}$$

chosen such that the work in a small motion is equal to $\mathbf{F}^{\text{ext}}\cdot\mathbf{U}$. The equilibrium equations – the statements that contact forces $\mathbf{f}$ balance load $\mathbf{F}^{\text{ext}}$ – is simply written with the tranposed rigidity matrix, as

$$\mathbf{F}^{\text{ext}} = {}^{\mathbf{T}}\underline{\underline{\mathbf{G}}}\cdot\mathbf{f}. \tag{15}$$

This is of course easily checked on writing down all force and moment coordinates, as well as the equilibrium form of stresses:

$$\Omega\Sigma_\alpha = \sum_{i<j} F^\alpha_{ij} r^\alpha_{ij}. \tag{16}$$

Given (11), (15) is equivalent to the theorem of virtual work, which states: For whatever vector of contact forces $\mathbf{f}$ that balance load $\mathbf{F}^{\text{ext}}$, *i.e.,* satisfying (15), and for whatever displacement vector $\mathbf{U}$ corresponding to relative contact displacements $\delta\mathbf{u}$ by (11), one has:

$$\mathbf{F}^{\text{ext}}\cdot\mathbf{U} = \mathbf{f}\cdot\delta\mathbf{u}.$$

As an example, matrices $\underline{\underline{\mathbf{G}}}$ and ${}^{\mathbf{T}}\underline{\underline{\mathbf{G}}}$ were written down in [47] in the simple case of one mobile disk with 2 contacts with fixed objects in 2 dimensions, the authors referring to $-{}^{\mathbf{T}}\underline{\underline{\mathbf{G}}}$ as the "contact matrix". The same definitions and matrices are used in [48] in the more general case of a packing of disks.

Returning to the case of small displacements associated with a load *increment* $\Delta\mathbf{F}^{\text{ext}}$, one may write, to first order in $\mathbf{U}$,

$$\Delta\mathbf{F}^{\text{ext}} = \underline{\underline{\mathbf{K}}}\cdot\mathbf{U}, \tag{17}$$

with a *total stiffness matrix* $\underline{\underline{\mathbf{K}}}$, comprising two parts, $\underline{\underline{\mathbf{K}}}^{(1)}$ and $\underline{\underline{\mathbf{K}}}^{(2)}$, which we shall respectively refer to as the *constitutive* and *geometric* stiffness matrices. $\underline{\underline{\mathbf{K}}}^{(1)}$ results from Eqns. 11, 12 and 15

$$\underline{\underline{\mathbf{K}}}^{(1)} = {}^{\mathbf{T}}\underline{\underline{\mathbf{G}}}\cdot\underline{\underline{\mathcal{K}}}\cdot\underline{\underline{\mathbf{G}}} \tag{18}$$

$\underline{\underline{\mathbf{K}}}^{(2)}$ is due to the change of the geometry of the packing, and is written down in Appendix B. Its elements, compared to their counterparts in $\underline{\underline{\mathbf{K}}}^{(1)}$, are of order $F/K_N R \sim h/R$, and therefore considerably smaller in all practical cases. The constitutive stiffness matrix is also called "dynamical matrix" [31, 49]. However the term "stiffness matrix" seems to us more appropriate, because this matrix has an important role in *static* problems and precisely expresses how *stiff* the mechanical response of the system is. One advantage of decomposition (18) is to separate out the effects of the contact constitutive law, contained in $\underline{\underline{\mathcal{K}}}$ and those of the contact network, contained in $\underline{\underline{\mathbf{G}}}$. $\underline{\underline{\mathbf{G}}}$ is sensitive in general to the orientations of normal unit vectors $\mathbf{n}_{ij}$ and to the "branch vectors" joining the grain centers to contact positions – which reduce to $R\mathbf{n}_{ij}$ for spheres of radius R. ($\underline{\underline{\mathbf{K}}}^{(2)}$, on the other hand, unlike $\underline{\underline{\mathbf{G}}}$, is sensitive to the curvature of grain surfaces at the contact point [50, 51]).

2. *Properties of the rigidity matrix*

To the rigidity matrix are associated the concepts (familiar in structural mechanics) of force and velocity (or displacement) indeterminacy, of relative displacement compatibility and of static admissibility of contact forces.

The degree of displacement indeterminacy (also called degree of hypostaticity in [32]) is the dimension k of the kernel of $\underline{\underline{\mathbf{G}}}$, the elements of which are displacements vectors $\mathbf{U}$ which do not create relative displacements in the contacts, $\delta\mathbf{u} = 0$. Such displacements are termed (first-order) mechanisms. Depending on boundary conditions, a grain packing might have a small number k_0 of "trivial" mechanisms, for which the whole system moves as one rigid body. In our case, attributing common values of $\tilde{\mathbf{u}}$ to all grains gives $k_0 = d$ independent global rigid motions.

A load vector $\mathbf{F}^{\text{ext}}$ is *supportable* if one can find a contact force vector $\mathbf{f}$ to balance it (such $\mathbf{f}$ is said to be *statically admissible* with $\mathbf{F}^{\text{ext}}$). In other words, $\mathbf{F}^{\text{ext}}$ should belong to the range of ${}^{\mathbf{T}}\underline{\underline{\mathbf{G}}}$, which is equivalent to being orthogonal to the kernel of $\underline{\underline{\mathbf{G}}}$. Supportable loads are those which do not work in mechanism displacements.

The *degree of force indeterminacy* H (also called degree of hyperstaticity in [32]) is the dimension of the kernel of ${}^{\mathbf{T}}\underline{\underline{\mathbf{G}}}$, or the number of independent self-balanced contact force vectors. If the coordinates of $\mathbf{f}$ are regarded as the unknowns in system of equations (15), and if $\mathbf{F}^{\text{ext}}$ is supportable, then there exists a whole H-dimensional affine space of solutions.

A dN_c-dimensional vector $\delta\mathbf{u}$ is a set of *compatible relative displacements* if one can find a displacement vector $\mathbf{U}$ such that the corresponding relative displacement vector is $\delta\mathbf{u}$, or in other words if it belongs to the range of $\underline{\underline{\mathbf{G}}}$. This is equivalent to being orthogonal to all elements of the kernel of ${}^{\mathbf{T}}\underline{\underline{\mathbf{G}}}$, the vectors of self-balanced contact forces.

From the relation between the rank of an operator and

the dimension of its kernel one deduces a general relation between H and k:

$$N_f + \mathrm{H} = dN_c + k. \tag{19}$$

An *isostatic packing* is defined as one devoid of force and velocity indeterminacy (apart from trivial mechanisms). Excluding trivial mechanisms (thus reducing N_f to $N_f - k_0$), and loads that are not orthogonal to them, one then has a square, invertible rigidity matrix. To any load corresponds a unique set of equilibrium contact forces. To any vector of relative contact displacements corresponds a unique displacement vector.

With frictionless objects, in which contacts only carry normal forces, it is appropriate to define N_c-dimensional contact force and relative displacement vectors, containing only normal components, and define the rigidity matrix accordingly [32]. Then (19) should be written as

$$N_f + \mathrm{H} = N_c + k. \tag{20}$$

In the case of frictionless spherical particles, all rotations are mechanisms, hence a contribution $nd(d-1)/2$ to k. Thus one may in addition ignore all rotations, and subtract $nd(d-1)/2$ both from N_f and from k, so that (20) is still valid. In such a case, the rigidity matrix coincides (up to a sign convention and normalization of its elements) with the one introduced in central-force networks, trusses and tensegrity structures (see *e.g.*,[52]), while Donev *et al.*, in a recent publication on sphere packings [53], call rigidity matrix what we defined as its transpose $^{\mathbf{T}}\underline{\underline{\mathbf{G}}}$.

D. Control parameters

The geometry and the mechanical properties of sphere packings under given pressure P depends on a small set of control parameters, which can be conveniently defined in dimensionless form [23, 54].

Such parameters include friction coefficient μ and viscous dissipation parameter ζ, which were introduced in Sec. II A.

The elastic contact law introduces a *dimensionless stiffness parameter* κ, which we define as:

$$\kappa = \left(\frac{\tilde{E}}{P}\right)^{2/3}. \tag{21}$$

Note that κ does not depend on bead diameter a. Under pressure P, the typical force in a contact is of order Pa^2. It corresponds to a normal deflection h such that $Pa^2 \sim \tilde{E}\sqrt{a}h^{3/2}$ due to the Hertz law (1). Therefore, κ sets the scale of the typical normal deflection h in Hertzian contacts, as $h/a \sim 1/\kappa$.

In the case of monodisperse sphere packings in equilibrium in uniform state of stress $\underline{\underline{\sigma}}$, pressure $P = \mathrm{tr}\underline{\underline{\sigma}}/3$ is linked to the average normal force $\langle N\rangle$ in the contacts by an exact relation. Let us denote as Φ the solid fraction and z the coordination number ($z = 2N_c/n$). As a simple consequence of the classical formula for stresses recalled in Sec. II B (Eqn. 8 in the static case, or Eqn. 16), one has, neglecting contact deflections before diameter a,

$$P = \frac{z\Phi\langle N\rangle}{\pi a^2}, \tag{22}$$

whence an exact relation between P and contact deflections:

$$\frac{\langle h^{3/2}\rangle}{a^{3/2}} = \frac{\pi}{z\Phi\kappa^{3/2}}.$$

The limit of rigid grains is approached as $\kappa \to \infty$. κ can reach very high values for samples under their own weight, but most laboratory results correspond to levels of confining pressure in the 100 kPa range, and very few experimental data are available on the mechanical properties of granular materials in quasistatic conditions below a few tens of kPa are available (see, however, [55] and [56]). This is motivated by engineering applications (100 kPa is the pressure below a few meters of earth), and this also results from difficulties with low confining stresses. Below this pressure range, stress fields are no longer uniform, due to the influence of the sample weight, and elastic waves are too strongly damped for their velocity to be measured.

In our simulations we set our lowest pressure level for the simulation of glass beads to 1 kPa or 10 kPa. Those values respectively correspond to $\kappa \simeq 181000$ and $\kappa \simeq 39000$ with the elastic properties of glass. On the one hand, upon increasing P, the entire experimental pressure range can be explored. On the other hand, we will check in Sections III, IV that these values of κ are high enough for some characteristic properties of rigid sphere packings to be approached with good accuracy.

Another parameter associated with contact elasticity is the ratio of tangential to normal stiffnesses (constant in our model), related to the Poisson ratio of the material the grains are made of. Although we did not investigate the role of this parameter, several numerical studies [49, 57] showed its influence on global properties to be very small.

The "mass" M of the global degrees of freedom is chosen to ensure slow and gradual changes in cell dimensions, and dynamical effects are consequently assessed on comparing the strain rate $\dot{\epsilon}$ to intrinsic inertial times, such as the time needed for a particle of mass m, initially at rest, accelerated by a typical force Pa^2, to move on a distance a. This leads to the definition of a *dimensionless inertia parameter* :

$$I = \dot{\epsilon}\sqrt{m/aP}. \tag{23}$$

The quasistatic limit can be defined as $I \to 0$. I was successfully used as a control parameter in dense granular shear flows [58, 59, 60], which might be modelled on writing down the I dependence of internal friction and density [61, 62].

In the following we will assess the influence of parameters μ, κ, I and ζ on sample states and properties. The sensitivity to dynamical parameters I and ζ should be larger in the assembling stage (as studied in the present paper) than in the subsequent isotropic compression of solid samples studied in paper II [37], for which one attempts to approach the quasi-static limit. Equilibrium configurations are then expected to depend on κ and μ only.

III. LOW-PRESSURE ISOTROPIC STATES OF FRICTIONLESS PACKINGS.

Numerical samples are most often produced by compression of an initially loose configuration (a granular gas) in which the grains do not touch. If the friction coefficient is set to zero at this stage, one obtains dense samples, which depend very little on chosen mechanical parameters. These frictionless configurations are in a particular reference state which was recently investigated by several groups [31, 53], and exhibit specific properties which are studied in the present Section. We shall dwell on such an academic model as assemblies of rigid or slightly deformable *frictionless* spheres in mechanical equilibrium for several reasons. First, we have to introduce various characterizations of the microstructure of sphere packings that will be useful in the presence of friction too. Then, such systems possess rather specific properties, which are worth recalling in order to assess whether some of them could be of relevance in the general case. Frictionless packings also represent, as we shall explain, an interesting limit case. Finally, one of our objectives is to establish the basic uniqueness, in the statistical sense, of the internal state of such packings under isotropic, uniform pressures, provided crystallization is thwarted by a fast enough dissipation of kinetic energy. We shall therefore compare our results to published ones whenever they are available. Specifically, we shall repeatedly refer to the works of O'Hern, Silbert, Liu and Nagel [31], and of Donev, Torquato and Stillinger [53], hereafter respectively abbreviated as OSLN and DTS. Both are numerical studies of frictionless sphere packings under isotropic pressures.

OSLN use elastic spheres, with either Hertzian or linear contact elasticity. They control the solid fraction Φ, and record the pressure at equilibrium. Their samples (from a few tens to about 1000 spheres) are requested to minimize elastic energy at constant density. For each one, pressure and elastic energy vanish below a certain threshold packing fraction Φ_0, which is identified to the classical random close packing density. Above Φ_0, pressure and elastic constants are growing functions of density. OSLN report several power law dependences of geometric and mechanical properties on $\Phi - \Phi_0$ which we shall partly review.

DTS differ in their approach, as unlike OSLN (and unlike us) they use strictly rigid spherical balls, and approach the density of equilibrated rigid, frictionless sphere packing *from below*. They use a variant of the classical (event-driven) hard-sphere molecular dynamics method [43, 63], in which sphere diameters are continuously growing, the Lubachevsky-Stillinger (LS) algorithm [64, 65], to compress the samples. DTS's approximation of the strictly rigid sphere packing as the limit of a hard sphere glass with very narrow interstices (gaps) between colliding neighbors (contact forces in the static packing are then replaced by transfers of momentum between neighbors), and their resorting to linear optimization methods [32, 66], enable them to obtain very accurate results in samples of 1000 and 10000 beads.

DTS expressed doubts as to whether numerical "soft" (elastic) sphere systems could approach the ideal rigid packing properties, and both groups differ in their actual definition of *jamming* and on the relevance and definition of the *random close packing* concept. Relying on our own simulation results, we shall discuss those issues in the following.

Our numerical results on packings assembled without friction are based on five different configurations of $n = 4000$ beads prepared by compression of a granular gas without friction. First, spheres are placed on the sites of an FCC lattice at packing fraction $\Phi = 0.45$ (below the freezing density, $\Phi \simeq 0.49$ [67]). Then they are set in motion with random velocities, and left to interact in collisions that preserve kinetic energy, just like the molecules of the hard-sphere model fluid studied in liquid state theory [43, 67]. We use the traditional event-driven method [63], in a cubic cell of fixed size, until the initial crystalline arrangement has melted. Then, velocities are set to zero, and the molecular dynamics method of Section II is implemented with an external pressure equal to 10 kPa for glass beads ($\kappa \simeq 39000$). Energy is dissipated thanks to viscous forces in contacts, and the packing approaches an equilibrium state. Calculations are stopped when the net elastic force on each particle is below $10^{-4}a^2P$, the elastic contributions to the stress components equal the prescribed value P with relative error smaller than 10^{-4} and the kinetic energy per particle is below $10^{-8}Pa^3$. On setting all velocities to zero, it is observed that the sample does not regain kinetic energy beyond that value, while the unbalanced force level does not increase. We have thus a stable equilibrium state. This is further confirmed by the absence of mechanism in the force-carrying contact network, apart from the trivial free translational motion of the whole set of grains as one rigid body. From (18), mechanisms naturally coincide with "floppy modes" of the constitutive stiffness matrix $\underline{\underline{\mathbf{K}}}^{(1)}$, while the geometric stiffness $\underline{\underline{\mathbf{K}}}^{(2)}$, as checked in Appendix B, is a very small correction (compared to those of $\underline{\underline{\mathbf{K}}}^{(1)}$ the elements of matrix $\underline{\underline{\mathbf{K}}}^{(2)}$ are of order κ^{-1}).

In the following, such configurations assembled without friction will be referred to as (κ-dependent, as some further compressions will also be investigated) A states. Observed geometric and mechanical characteristics of A

states are reported below and compared to other published results, in particuler those of OSLN and DTS. We also state specific properties of *rigid* frictionless sphere packings, to which A configurations at high κ are close. Unlike OSLN, we use pressure or stiffness level κ as the control parameter. The state OSLN refer to as "point J", which appears as a rigidity threshold $\Phi = \Phi_0$ if solid fraction Φ is used as the control parameter, is approached here as $\kappa \to \infty$.

A. Energy minimization and density

In spite of a long tradition of studies on the geometry of sphere assemblies, the connection between mechanical equilibrium and density maximization has seldom been stressed. It is worth recalling it here, as the purpose of this work is to discuss both geometric and mechanical properties of such particle packings. This connection is simply expressed on noting that configurations of rigid, frictionless, non-adhesive spherical particles in stable equilibrium under an isotropic confining pressure are those that realize a local minimum of volume in configuration space, under the constraint of mutual impenetrability. It is no wonder then that the isotropic compaction of frictionless balls is often used as a route to obtain dense samples [27, 30].

This property was presented, in slightly different forms, in the mathematics [68] and physics [32, 53] literature. We briefly recall its derivation here, because of its importance, and state it in a form adapted to our specific boundary conditions. First, let us assume we have an equilibrium state in which compressive normal contact forces between n rigid spherical balls, which are contained in the periodic, deformable cell defined in Section II, balance the external load. It is convenient to use the notations of Sec. II C, and to choose the given configuration as reference, with volume Ω_0 and displacements equal to zero by definition. The load vector $\mathbf{F}^{\text{ext}}$ has only three non-zero coordinates, equal to $\Omega_0 P$: those corresponding to the cell degrees of freedom. Let us show that the potential energy $W = P\Omega$ is locally minimized in configuration space. For any small displacement vector $\mathbf{U}$ (dealt with as if it were infinitesimal) its first-order variation is, by the theorem of virtual work (applied in the frictionless case)

$$\Delta W = -\Omega_0 P \sum_\alpha \epsilon_\alpha = -\sum_{i<j} N_{ij} \delta u_{ij}^N.$$

The sum runs over all pairs i, j in contact with $N_{ij} > 0$, and ϵ_α, as in (9), are coordinates of $\mathbf{U}$. If the impenetrability constraints are not violated, then $\delta u_{ij}^N \leq 0$: touching grains should part rather than overlap. Thus $\Delta W \geq 0$, and $\Delta W = 0$ is only possible for those displacement vectors such that $\delta \mathbf{u}_{ij} = 0$ in all contacts carrying a non-zero force. Such displacement vectors are mechanisms on the backbone (force-carrying network) of the packing. It was shown in [32] that there cannot exist such mechanisms if the equilibrium state is stable. Otherwise the work of external forces would entail a net gain of kinetic energy in such a motion, which would not be compensated by contact forces, since they do not work in that case.

Conversely, if we assume that the current configuration is a local minimum of W under impenetrability constraints, there should exist a set of Lagrange multipliers $N_{ij} \geq 0$ defined for all grain pairs, with $N_{ij} \neq 0$ only for pairs in contact (where the impenetrability constraint is active), such that, for any k, $1 \leq k \leq n$, and α, $1 \leq \alpha \leq 3$

$$\begin{aligned} \frac{\partial W}{\partial \tilde{u}_k^{(\alpha)}} &= 0 = \sum_{1 \leq i < j \leq n} N_{ij} \frac{\partial h_{ij}}{\partial \tilde{u}_k^{(\alpha)}} \\ \frac{\partial W}{\partial \epsilon_\alpha} &= -\Omega_0 P = \sum_{1 \leq i < j \leq n} N_{ij} \frac{\partial h_{ij}}{\partial \epsilon_\alpha} \end{aligned} \tag{24}$$

The sum in the r.h.s. of (24) can be written only with the list of N_c contacts, and, as the increase in particle overlap h_{ij} is the normal part of the relative displacement at contact, the partial derivatives are the corresponding elements of the matrix $\underline{\underline{\mathbf{G}}}$ associated with the contact network. Therefore, if $\mathbf{F}^{\text{ext}}$ is the load vector with all coordinates equal to zero except the three last ones, equal to $\Omega_0 P$, if $\mathbf{N}$ denotes the N_c-dimensional vector of coefficients N_{ij}, then (24) simply reads

$$\mathbf{F}^{\text{ext}} = {}^{\mathbf{T}}\underline{\underline{\mathbf{G}}} \cdot \mathbf{N},$$

which shows that this vector can be viewed as a set of normal contact forces balancing the load. Any configuration realizing a local volume minimum under impenetrability constraints in configuration space is therefore a mechanical equilibrium state for an isotropic pressure, with only normal forces in the contacts. Mechanisms on the backbone are excluded because they would allow for a nonzero volume decrease.

In DTS [53] and in other works by the same group [66, 69], the authors use a definition of *strictly jammed* configurations of hard particles as those for which particles cannot move without interpenetrating or increasing the volume of the whole system. Their definition is therefore exactly equivalent to that of a stable equilibrium state with rigid, frictionless grains under an isotropic confining pressure.

We now turn to elastic, rather than rigid, spherical particles, with Hertzian contacts as defined in Sec. II. Then stable equilibrium states under given pressure P are local minima of the potential energy defined as (H denotes the Heavside step function)

$$W = P\Omega + \sum_{1 \leq i < j \leq n} \frac{2\tilde{E}\sqrt{a}}{15} h_{ij}^{5/2} H(h_{ij}). \tag{25}$$

As stiffness parameter κ increases, the second term of (25) imparts an increasing energetic cost to elastic

deflections h_{ij}, and the solution becomes an approximation to a minimum of the first term, with impenetrability constraints, *i.e.,* a stable equilibrium state of rigid, frictionless balls. The value of κ is an indicator of the distance to the ideal, rigid particle configuration, and it is arguably more convenient to use that the density, used by OSLN, because it does not vary between different samples. OSLN had to adjust the density separately for each sample in order to approach the limit of rigid grains, so that the pressure approached zero, corresponding to a rigidity threshold.

Our A configurations have a solid fraction $\Phi = 0.6370 \pm 0.0015$ (indicated error bars correspond throughout the paper to one sample-to-sample standard deviation). OSLN performed a careful statistical analysis of finite size effects and uncertainty on Φ, with which our results are clearly in good agreement, as apparent on Fig. 1. Fig. 1 also shows another data point for $n = 1372$. Our Φ values fall within OSLN's estimation of size-dependent averages and fluctuations, once it is extrapolated to larger sample sizes. We shall check below that the small density difference between $\kappa = 39000$ and $\kappa \to \infty$ is much smaller than the statistical uncertainty on Φ. DTS focus on force-carrying network and

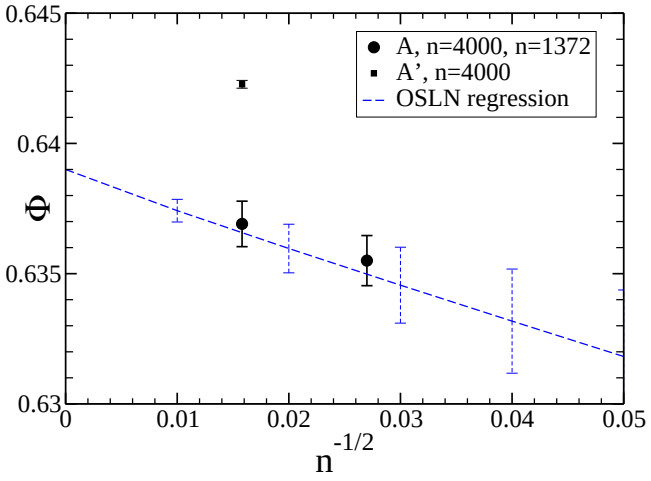

FIG. 1: (Color online) Solid fraction Φ versus $n^{-1/2}$. Blue dotted line: average value, with standard deviation indicated as error bars, according to OSLN's results, extrapolated to $n \to \infty$. Black round dots with error bars: our A samples for $n = 4000$ and other, very similar results for $n = 1372$. Square dot: A' samples with $n = 4000$ (this point has a smaller error bar).

pair correlations. They do not report Φ values very precisely, but mention solid fractions in the range 0.625 to 0.63 (page 7 of [53]), on excluding the volume of particles that transmit no force. This apparently entails $\Phi \geq 0.64$ once those inactive grains, which represent about 2.2% of the total number, are taken into account. This could be explained by the influence of the compression rate in the assembling stage on the structure and density of dense packings. Slower compressions, in which the system is agitated at lower densities for some time, might lead to better ordered configurations, which have started to evolve towards the thermodynamically stable FCC crystalline arrangement. As OSLN directly used constant volume static routes from an initial configuration to a nearby elastic energy minimum (conjugate-gradient minimization), their procedure is expected to be the fastest, and involves no particle agitation. This interpretation is supported by some other data we have obtained on another, similar sample series, denoted as A', for which (the initial motivation being to save computation time) the LS algorithm was used to bring the solid fraction from 0.45 to 0.61, before equilibrating at the desired pressure with Hertzian sphere molecular dynamics. The LS procedure, in which particle diameters grow at a prescribed rate, thereby increasing density, unavoidably involves many collisions and a considerable level of agitation. In practice, kinetic energy actually increases: receding velocities after collision should be artificially increased in order to make sure particles that are continuously growing in diameter actually move apart after colliding [64, 65]. It has to be scaled down now and then for computational convenience, a feature the actual compacting process, depending on the ratio of growing rate to quadratic velocity average, is sensitive to. In our implementation there were typically 110 collisions per sphere in the range $0.49 \leq \Phi \leq 0.58$ (the most dangerous interval for crystal nucleation [67, 70]), and 90 collisions for $0.58 \leq \Phi \leq 0.61$. LS-made samples were shown in [10] to jam, depending on the compression rate, over the whole solid fraction range between 0.64 and the maximum value $\pi/(3\sqrt{2})$ corresponding to the perfect FCC crystal. Our A' samples exhibit slightly higher densities than A ones, $\Phi = 0.6422 \pm 0.0002$ (see Fig. 1). DTS report using expansion rates of 10^{-4}, while ours started as 10^{-2} in units of the quadratic mean velocity, and somewhat higher densities than our A' values are therefore to be expected. Further below we present a geometric characterization of A and A' configurations, showing that A' ones are closer to crystallization by a small, but systematic increment of usual order parameters.

Molecular dynamics is not the fastest conceivable route to minimize the sum of elastic and potential energies, and the MD approach does not necessarily find the nearest minimum in configuration space. However, the time scales involved can be compared to experimental ones. In simulations, A configurations approach their final density within a few tens of time $\tau = \sqrt{m/(aP)}$, and come to their final equilibrium with a few hundreds of τ. Comparable laboratory experiments in which dense samples are assembled are sample preparation with the pluviation or rain deposition technique, in which grains are deposited at constant flow rate under gravity, with a constant height of free fall [33, 34, 71, 72]. Such an assembling technique produces homogeneous samples. Grains are first agitated near the free surface, and then subjected to a quasi-static pressure increase as pouring procedes. The relevant pressure scale corresponds therefore to the

weight of the agitated superficial layer of the sample being assembled [71], typically of the order of 10 diameters, hence $P \sim 10mg/a^2$ and $\tau \sim \sqrt{a/(10g)}$, about 3×10^{-3} s for $a = 1$ mm. Approximating the compaction time by the time needed to renew entirely the agitated superficial layer, we obtain a few times 10^{-2} s if this time is to be of order 10τ, as in our simulations. This corresponds to a fraction of a second to fill up a 10 cm high container, a value within the experimental range. The main conclusion from this crude analysis is that laboratory assembling processes are rather fast, with typical compaction times similar to those of our simulated isotropic compression procedure.

B. Isostaticity, coordination number and rattlers.

We now turn our attention to another specific property of equilibrium states of rigid, frictionless spheres, and show how it influences high κ configurations as well. In the language of OSLN, "point J" (the limiting, rigid state) "controls its vicinity", and we shall show that several of their observations of power laws can be directly ascribed to the particular properties of the force-carrying structure.

Several authors have predicted, observed or discussed the *isostaticity property* [32, 73, 74, 75, 76, 77, 78, 79] and we recall it here in order to exploit some of its consequences. Isostaticity is a property of the *backbone* or force-carrying contact network in equilibrium packings of rigid, frictionless spheres. It means that such networks are both devoid of hyperstaticity (force indeterminacy) and of hypostaticity (displacement indeterminacy), apart from possible trivial motions in which all force-carrying grains move as one rigid body. These two properties have different origins [32], and are not valid under the same assumptions. While the absence of hyperstaticity ($\mathrm{H} = 0$ with the notations of Sec. II C) results from the generic disorder of the packing geometry and would hold true for arbitrarily shaped rigid particles interacting by purely normal contact forces whatever the sign of those forces, the absence of hypostaticity property (except trivial mechanisms, $k = k_0$) only applies to *spherical* particles with *compressive* forces in the contacts. While the lack of hyperstaticity applies to the whole packing, the absence of non-triavial mechanism motion is a property of the backbone only. This distinction highlights the role of the *rattlers*, defined as the grains that do not participate in carrying forces (and remain, therefore, free to "rattle" within the cage formed by their force-carrying, rigidly fixed neighbors). The absence of force indeterminacy applies to the *contact structure*, and remains true if the rattlers come into contact with one or several force-carrying grains. The non-existence of non-trivial mechanisms, is a property of the *backbone* and applies to the set of spheres that carry non-vanishing forces exclusively. Our A samples at $\kappa = 39000$ have a proportion $x_0 = 0.013 \pm 0.002$ of rattlers. Distinguishing between the backbone and the rattlers requires some care, as very small forces on the backbone might be confused with forces below tolerance between rattler and backbone grains, or between two rattlers. We apply the following simple procedure. First, we regard as rattlers all spheres having less than four contacts: less than three contacts implies a mechanism, and only three is impossible if forces are all strictly compressive. We also discard from the backbone all spheres with only forces smaller than the tolerance. Then, all the contacts of eliminated spheres being also removed, other spheres might (although this is an extremely rare occurrence) have less than four contacts, so the procedure is iterated (twice at most is enough in our samples, although one such sweep is usually enough) until no more rattler is detected. We found this method to work correctly for $n = 4000$ and $\kappa = 39000$. If one eliminates too many particles, the identified backbone might become floppy (hypostatic). As we compute and factorize its constitutive stiffness matrix, we could check that it was indeed positive definite, and this pitfall was therefore avoided. The proportion of rattlers is likely to increase for stiffer contacts (higher κ values). The contact coordination number, as a consequence of the isostaticity property, should be equal to 6 in the rigid limit *on the backbone*. If N_c is the number of *force-carrying* contacts, we define the global coordination number as $z = \dfrac{2N_c}{n}$ (thereby discarding possible contacts of the rattlers), and the backbone coordination number as $z^* = \dfrac{2N_c}{n(1-x_0)} = \dfrac{z}{1-x_0}$. z^*, rather than z, has the limit 6 as $\kappa \to +\infty$. A samples ($\kappa = 39000$) have $z^* = 6.074 \pm 0.002$ (and hence $z \simeq 5.995$), the excess over the limit $z^* = 6$ resulting from contacts that should open on further decreasing the pressure.

We now use the isostaticity property to evaluate the density increase due to finite particle stiffness. To first order in the small displacements between $P = 0$ (or $\kappa = +\infty$) and the current finite pressure state A, one might use the theorem of virtual work recalled in Section II C, with the displacements that bring all overlaps h_{ij} to zero, and the current contact forces. Such motions leading to a simultaneous opening ($h_{ij} = 0$) of all contacts are only possible on networks with no hyperstaticity, because there is no compatibility condition on relative normal displacements [32]. This yields an estimate of the increase of the solid fraction $\Delta\Phi$ over its value Φ_0 in the rigid limit, as

$$\frac{1}{\Omega}\sum_{ij} N_{ij} h_{ij} = P\frac{\Delta\Phi}{\Phi}. \tag{26}$$

This equality can be rearranged using the Hertz contact law (1) to relate N_{ij} to h_{ij}, and relation (22). We denote as $Z(\alpha)$ the moment of order α of the distribution of normal forces N_{ij}, normalized by the average over all contacts:

$$Z(\alpha) = \frac{\langle N^\alpha \rangle}{\langle N \rangle^\alpha}. \tag{27}$$

(26) can be rewritten as:

$$\Delta\Phi = 3^{5/3}\Phi^{1/3}Z(5/3)\left(\frac{\pi}{z}\right)^{2/3}\kappa^{-1}. \qquad (28)$$

As we observe $Z(5/3) = 1.284$, and taking for z and Φ the values at the highest studied κ ($\kappa = 39000$), this enables us to evaluate the density change between those configurations and the rigid limit as $\Delta\Phi \simeq 1.15 \times 10^{-4}$ (as announced before this is smaller than the statistical uncertainty on Φ). This provides us with a more accurate estimation of the solid fraction Φ_0 of the packing of rigid particles ($\kappa = +\infty$). Recalling $\kappa^{-1} = (P/\tilde{E})^{2/3}$, (28) means that the macroscopic relation between pressure and density has the same power law form ($P \propto (\Delta\Phi)^{3/2}$) as the contact law ($N \propto h^{3/2}$). This was observed by OSLN. It would hold, because of the isostaticity property in the rigid limit, for whatever exponent m in the contact law, the prefactor of the macroscopic relation $P \propto (\Delta\Phi)^m$ involving $Z(1 + 1/m)$, a moment of the geometrically determined force distribution.

Estimating Φ_0 as indicated above, we checked relation (28), and observed it to be satisfied (Fig. 2) provided the compression producing denser states is slow enough. Otherwise, a stepwise pressure increase in which samples temporarily depart from equilibrium, before restabilizing in a new configuration, can entail enough reshuffling to produce some additional density increase (typically of order $\delta\Phi \sim 10^{-3}$ in our samples). This phenomenon, albeit of lower importance, might be comparable to the agitation in the assembling stage, entailing the difference between states A and A'. It might also be due to the fluctuations of Φ_0 between different possible equilibrium configurations in a finite sample: some reshuffling caused by a perturbation enables the system to choose a different equilibrium state, which is denser because potential energy can only decrease. According to this second interpretation such a density increment should vanish in the large system limit, but we did not investigate this issue. It should be noted that relation (28), upon derivation, also links the bulk modulus $B = \Phi\frac{\partial P}{\partial \Phi}$, either to $\Delta\Phi$:

$$B = \frac{z\tilde{E}(\Phi_0\Delta\Phi)^{1/2}}{3^{3/2} \times 2\pi\left[Z(5/3)\right]^{3/2}}, \qquad (29)$$

thus explaining observations of such power laws by OSLN [31], or, equivalently, to P:

$$B = \frac{1}{2Z(5/3)}\left(\frac{z\Phi_0}{3\pi}\right)^{2/3}\tilde{E}^{2/3}P^{1/3}. \qquad (30)$$

Relation (30) does not involve $\Delta\Phi$, and is consequently not affected by possible perturbations entailing slight, but systematic density increments. (30) applies indeed as a very good approximation within a large pressure interval, as shown on Fig. 3. The sole knowledge of the random close packing solid fraction Φ_0, of the coordination number $z \simeq 6$ at low pressure and of the moment $Z(5/3)$ of the force distribution thus enables a quantitative prediction of the pressure dependence of the *bulk* modulus (down to $\kappa \sim 1000$ in terms of stiffness level). The *shear* modulus behaves differently, and anomalously in that case [31], and will be discussed in paper III [38].

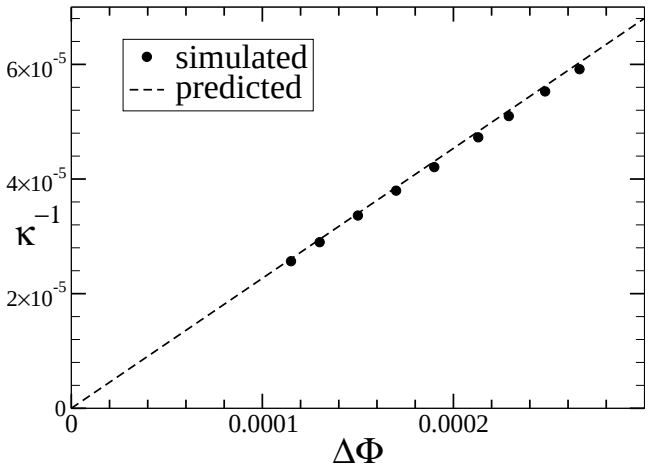

(a) Small $\Delta\Phi$, one sample.

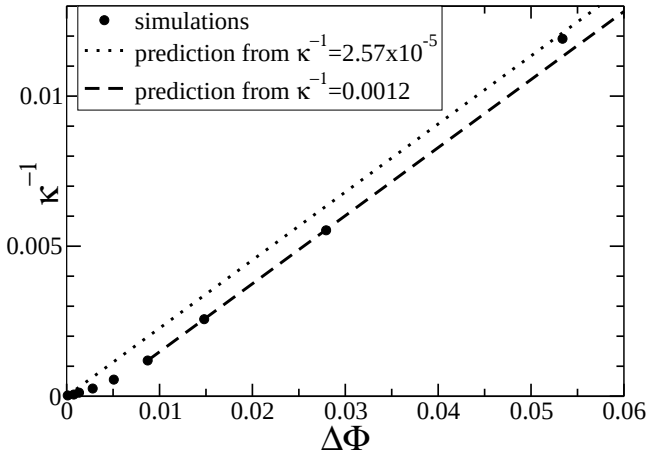

(b) Larger $\Delta\Phi$, average over 5 samples.

FIG. 2: $\kappa^{-1} = (P/\tilde{E})^{2/3}$ versus $\Delta\Phi$. Points: simulations. Dotted line: prediction according to (28), going through lowest P point by construction. (a): results for one sample slowly compressed towards slightly higher pressures. (b): results for compression steps (P increased by factors of $\sqrt{10}$ (as in paper II [37], note the different scale), averaged on 5 samples, showing larger density increases caused by agitation at low pressures. The formula actually works better on choosing a higher P value as a reference (lowest P point) to evaluate Φ_0.

C. Properties of force-carrying network

If, as an approximation, we ignore those contacts in excess over the minimum backbone, then the force distri-

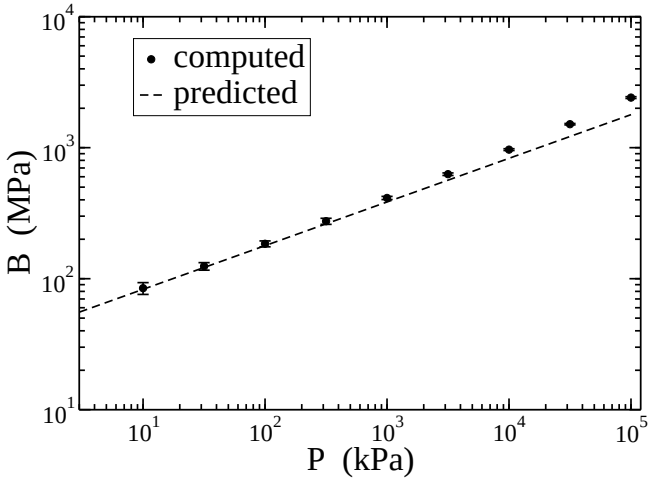

FIG. 3: Bulk modulus B versus isotropic confining pressure P for simulated frictionless glass beads. Note the very good agreement between computed values and formula (30) except for large pressures.

bution we observe in A samples at high κ values should coincide with the one of a rigid packing, which due to isostaticity is a purely *geometric* property. It is represented on Figure 4. The data presented here are averaged

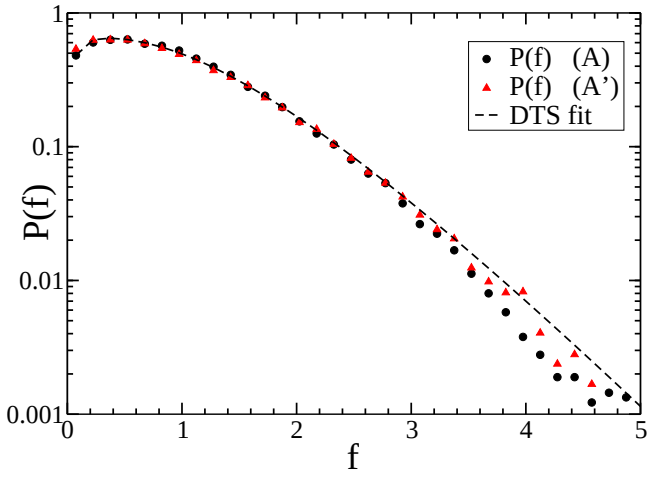

FIG. 4: (Color online) Probability distribution function $P(f)$ of normalized contact forces $f = N/\langle N\rangle$ in A and A' configurations at high κ. The dashed line is the fit proposed by DTS: $P(f) = (3.43f^2 + 1.45 - 1.18/(1 + 4.71f))\exp(-2.25f)$.

over 5 samples, which requires some comment in view of the remark by OSLN that the force probability distribution function $P(f)$ is "not self-averaging". Those authors showed that different results are obtained for $P(f)$ on either normalizing each force by the average force of the sample it belongs to, or by the average of all forces measured in all avalailable samples at the same density. Our procedure differs from theirs because we use pressure, rather than solid fraction, as the control parameter. Due to (22), all samples prepared at the same pressure have the same average force, and the "self-averaging" property is recovered. The choice of Φ as a state variable, because of the finite size of the sample causing fluctuations of the threshold Φ_0 where P vanishes, is less convenient in that respect.

Fig. 4 also shows that the form proposed by DTS to fit their data is in very good agreement with our results, except perhaps for large forces. The systematic difference in the fraction of rattlers ($x_0 \simeq 2.2\%$ reported by DTS) might stem to some extent from the different distance from the rigid state (as we did not attempt to equilibrate samples above $\kappa = 39000$), although the change of x_0 with Φ is slow (as observed by OSLN). The difference with the DTS value is probably rather due to the very slightly denser and more ordered states obtained by those authors. We note that A' configurations also had more rattlers ($x_0 \simeq 1.8\%$) than A ones, and that their force distribution is better fitted by the DTS formula for large values.

The presence of rattlers complicates the analysis of geometric properties of static packings, because their positions are not determined by the equilibrium requirement. The rattlers are free to move within a "cage" formed by their backbone neighbors, and there is no obvious way in principle to prefer one or another of their infinitely many possible positions. This renders the evaluation of geometric data like pair correlations somewhat ambiguous. Moreover, rattlers, although scarce in frictionless packings, can be considerably more numerous in frictional ones, as we shall see further below. We therefore specify in the results presented below whether they correspond to direct measurement on the configurations resulting from the simulations, with rattlers floating in some positions resulting from compaction dynamics, or whether rattlers have been fixed, each one having three contacts with the backbone (or some previously fixed other rattler). To compute such fixed rattler positions with MD, we regard each backbone grain as a fixed object, exert small isotropically distributed random forces on all rattlers and let them move to a final equilibrium position (assuming frictionless contacts). A third possibility is to eliminate rattlers altogether before recording geometric data. These are three choices referred to as I, II and III in the sequel, and we denote observed quantities with superscripts I, II or III accordingly. Frictionless packings under gravity, if locally in an isotropic state of stress, are expected to be in the same internal state and to exhibit the same properties as the ones that are simulated here. In such a situation, individual grain weights are locally, within an approximately homogeneous subsystem, dominated by the externally imposed isotropic pressure. There is no rattler, but some grains are simply feeling their own weight, or perhaps that of one or a few other grains relying on them. Such grains are those that would be rattlers in the absence of gravity. Instead of freely floating within the cage of their backbone neighbors, they are supported by the cage floor. The situation should therefore be similar to that of our samples after all rattlers have been put in

contact with the force-carrying structure (treatment II), except that the small external forces applied to them are all directed downwards. Table I gives the distribution of local coordination number values among the spheres for A and A' states at $\kappa = 39000$. If rattlers are fixed by

State	x_0	x_1	x_2	x_3	x_4	x_5	x_6	x_7	x_8	x_9	x_{10}	x_{11}
A (I)	1.3	0	0	0	11.1	23.2	28.4	22.6	10.3	2.8	0.3	0.02
A' (I)	1.8	0	0	0	11.6	22.5	28.2	22.3	10.6	2.8	0.3	0.01
A (II)	0	0	0	1.1	10.7	22.7	28.2	22.9	10.9	3.1	0.3	0.02
A' (II)	0	0	0	1.7	10.9	21.9	28.2	22.5	11.4	3.1	0.3	0.01

TABLE I: Percentages x_i of grains having i contacts in A and A' configurations, on ignoring the rare contacts with or between rattlers (I), or on fixing the rattlers onto the backbone with small (randomly oriented) forces (II).

three contacts to the backbone (method II), one records slightly changed proportions of spheres having $n \geq 3$ contacts, to which values observed within samples under gravity should be compared.

D. Pair correlations, geometry and order

Pair correlations should preferably be measured either with method I or method II, as there is no reason to eliminate rattlers before studying geometric properties. Comparisons between pair correlation functions $g^I(r)$ and $g^{II}(r)$ (Fig. 5) show very little difference on the scale of one particle diameter. Results of Fig. 5 are very similar to other published ones (*e.g.,* in DTS), with an apparent divergence as $r \to a$ and a split second peak, with sharp maxima at $r = a\sqrt{3}$ and $r = 2a$. The pair correlation

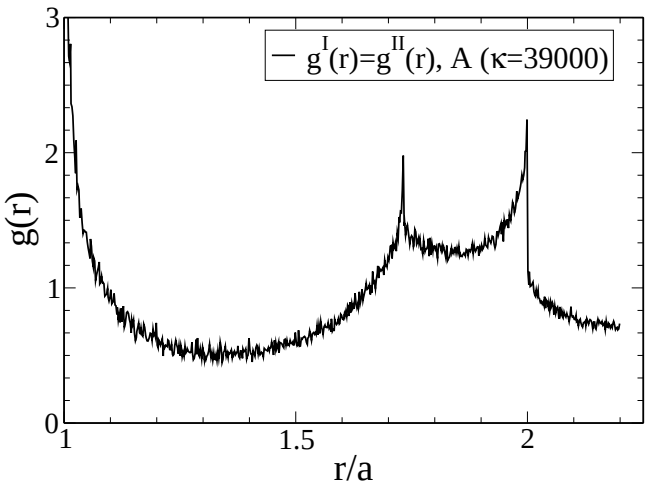

FIG. 5: Pair correlation functions $g^I(r)$ and $g^{II}(r)$ versus r/a in A samples at $\kappa = 39000$. Both definitions coincide on this scale (only the peak for $r \to a^+$ is slightly different).

function should contain a Dirac mass at $r = a$ in the limit of rigid grains, which broadens into a sharp peak for finite contact stiffness. The weight of this Dirac term or peak in the neighbor intercenter distance probability distribution function $4\pi\frac{n}{\Omega}r^2 g(r) = 24(r^2/a^3)\Phi g(r)$ is coordination number z, and the shape of the left shoulder of the peak at finite κ is directly related to the force distribution:

$$(\text{For } \delta > 0)\ g(a-\delta) = \frac{z a^3 \tilde{E}\sqrt{a\delta}}{48\Phi(a-\delta)^2} P(\frac{\tilde{E}\sqrt{a}\delta^{3/2}}{3}).$$

This explains the observation by OSLN [31] of the width of the $g(r)$ peak decreasing approximatively as $\Delta\Phi$, while its height increases as $(\Delta\Phi)^{-1}$, as the threshold density Φ_0 is approached from above: the form of the distribution of contact forces remains exactly the same for all small enough values of $\Delta\Phi$, with a scale factor proportional to $\Delta\Phi^{3/2}$, due to Eqns. 22 and 28.

As $r \to a^+$, pair correlations are conveniently expressed with the gap-dependent coordination number $z(h)$. $z(h)$ is the average number of neighbors of one sphere separated by an interstice narrower than h ($z(0)$ is the usual contact coordination number z). This function is represented on Fig. 6, with its possible different definitions z^I, z^{II} and z^{III}. $z^{III}(h)$ takes the value z^* for $h = 0$, and is very well fitted by the functional form used by DTS in Ref. [53]. $z(h)$ is bound to differ from its rigid limit for h of the order of the typical overlap $\kappa^{-1} = 2.6 \times 10^{-5}$. We observe $z(h) \propto h^{0.6}$ up to $h \simeq 0.3$ for all three definitions. The treatment of rattlers affects the prefactor, that of z^{III} approaching the one given in Ref. [53], where the same power law was observed. This corresponds to $g(r)$ diverging as $(r-a)^{-0.4}$ as $r \to a^+$.

The sharp drop of $g(r)$ at $r = a\sqrt{3}$ and $r = 2a$ is found by DTS to go to a discontinuity in the rigid particle limit. This can be understood as follows. Each sphere has a number of first contact neighbors (z on average) at distance $r = a$ if the grains are rigid, and a number of second contact neighbors (*i.e.* particles not in contact with it, but having a contact with at least one of its first contact neighbors). Such second contact neighbors will make up for a significant fraction of particles with their centers at a distance $r \leq 2a$, but none of them can be farther away. Futhermore, this leads to a systematic depletion of the corona $2a < r < 2a + \delta$ (with $0 < \delta < a$) by steric exclusion.

The backbone is best studied with method III, ignoring rattlers. One may then record the density of specific particle arrangements. We thus find the contact network (joining all centers of interacting particles by an edge) to comprise a number of equilateral triangles, such that on average each backbone grain belongs to 2.04 ± 0.04 triangles. In the rigid limit this gives a Dirac term for $\theta = \pi/3$ in the distribution of angles θ between pairs of contacts of the same grain. Tetrahedra are however very scarce (as observed by DTS), involving about 2.5% of the beads, and pairs of tetrahedra with a common triangle are exceptional (5 such pairs in 5 samples of 4000 beads). Pairs of triangles sharing a common base are present with a finite density, which explains the discontinuous drop at

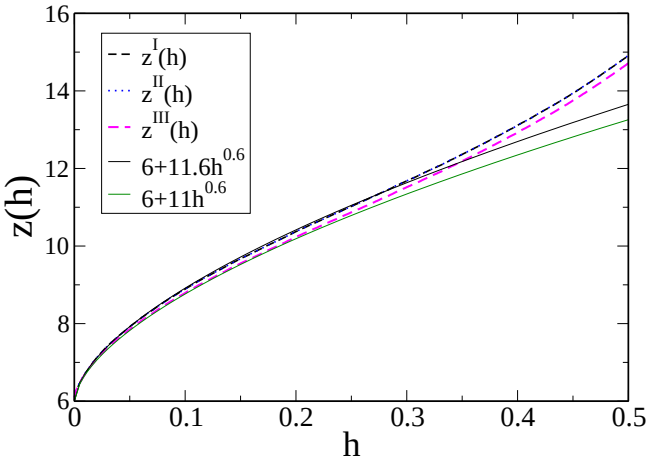

(a) Linear scale.

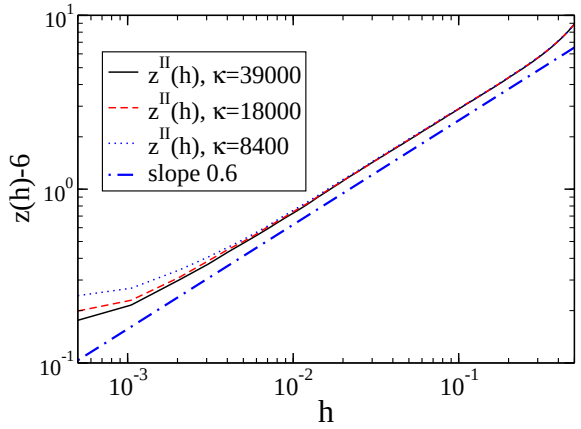

(b) $z^{II}(h) - 6$, logarithmic scale.

FIG. 6: (Color online) Coordination number of near neighbors function of interstice h. Different definitions z^I, z^{II} and z^{III} according to treatment of rattlers (see text).

$r = a\sqrt{3}$ of $g(r)$, this being the largest possible distance for such a population of neighbor pairs.

A recurring issue in sphere packing studies is the possible presence of crystal nuclei, the FCC and HCP lattices (the former the more stable thermodynamically) and hybrids thereof being the densest possible arrangements. A recent numerical study of crystallization dynamics in the hard sphere fluid is that of Volkov *et al.* [67], in which the authors used several indicators and measures of incipient crystalline order that we apply here to A and A' states. First, *bonds* are defined as (fictitious) junctions between the centers of neighboring spheres if their distance is smaller than some threshold, often chosen as corresponding to the first minimum in $g(r)$ (about $1.4a$ in our case). Then, a *local* order parameter is associated to each grain i, as:

$$Q_l^{\rm loc}(i) = \left[\frac{4\pi}{2l+1} \sum_{m=-l}^{m=l} |\hat{q}_{lm}(i)|^2 \right]^{1/2}, \qquad (31)$$

in which $\hat{q}_{lm}(i)$ is an average over all neighbors j of i numbered from 1 to $N_b(i)$, the number of bonds of i:

$$\hat{q}_{lm}(i) = \frac{1}{N_b(i)} \sum_{j=1}^{N_b(i)} Y_{lm}(\mathbf{n}_{ij}), \qquad (32)$$

$\mathbf{n}_{ij}$ denoting as usual the unit vector pointing from the center of i to the center of j.

Q_4 and Q_6, in particular, have been used to distinguish different local orders [7, 67, 70]. In the sequel we use the average $Q_6^{\rm loc}$ of (32) over all grains, as well as a global parameter Q_6, defined on taking the average over all bonds within the sample, instead of those of a particular grain i in (31). The values of those parameters are given in table II. Global Q_6 values are small in large samples, because they tend to average to zero in the presence of randomly oriented polycrystalline textures. They can be used nevertheless to observe crystallization in samples of $\sim$ 10000 beads, as they finally reach values comparable to the perfect crystal one [70].

Next, following [67], we normalize the set $(\hat{q}_{lm}(i))_{l\le m\le m}$, on multiplying, for any given l and i, each of its $2l+1$ components by an appropriate common factor thus obtaining $(\overline{q}_{lm}(i))_{l\le m\le m}$, such that

$$\sum_{m=-l}^{m=l} |\overline{q}_{lm}(i)|^2 = 1. \qquad (33)$$

If the values $\hat{q}_{lm}(i)$ are viewed as the components of a $2l+1$-dimensional local order parameter, then $\overline{q}_{lm}(i)$ might be viewed as its "phase" or "angular" part, characteristic of the choice of a direction, rather than of the intensity or extent with which the system is locally ordered. Then a bond is termed *crystalline* if it joins two particles for which those "phases" are sufficiently correlated: (the star indicates complex conjugation)

$$\left| \sum_{m=-l}^{m=l} \overline{q}_{lm}(i) \overline{q}^*_{lm}(j) \right| \ge 0.5. \qquad (34)$$

A particle is said to be in a *crystalline configuration* if at least 7 of its bonds (out of 12.5-13, see table II)) is "crystalline", according to definition (34) with $l = 6$. One may check how numerous those particles are and whether they tend to cluster in crystalline regions. Table II contains those various indicators, as observed in samples of type A and A' at the largest studied stiffness level. Order parameters have a very small value, indicating as expected a large distance to crystal order. Only a small fraction of

bonds and grains are declared "crystalline" according to the above definitions. However, it does transpire from the data of table II that A' states are consistently more "ordered" than A ones, with a small, but systematic difference for all listed indicators (see also Appendix D). Only traces of crystalline order, from table II, are present in the disordered systems studied here. Direct visualization of "crystalline" regions show, however, some local tendency to organization in parallel stacked layers, and to the formation of 2D triangular lattice patterns within the layers, as apparent on the example of Fig. 7. Luchnikov *et al.* [70] report simulation of 16000 particle samples of the hard sphere fluid evolving towards crystallization at constant density (between $\Phi = 0.55$ and $\Phi = 0.6$), as monitored by the global Q_6 parameter and the distribution of local Q_6 values. They observed, like Volkov *et al.* [67], that several thousands of collisions per particle were necessary for a significant evolution to take place, which is compatible with our observation of a detectable, but very small tendency with about 100 collisions per particle with our A' samples.

$Q_6^{\rm loc}$ and $Q_4^{\rm loc}$, as defined in (31), were also used by Aste *et al.* [7] to characterize local arrangements, in an experimental study of sphere packing geometry by X-ray tomography. These results rely on observations of large samples of tens to hundreds of thousands of beads, although not isotropic. Particles are classified according to the pair of values $Q_6^{\rm loc}(i)$, $Q_4^{\rm loc}(i)$. We compared the geometry of our numerical samples of similar density to those experimental data, with the result that although the most frequently observed values of $Q_6^{\rm loc}(i)$ and $Q_4^{\rm loc}(i)$ were quite close to experimental ones in dense samples, and the proportion of hcp-like particles were similar, fcc-like local environments were exceptional in simulations, whereas a few percent of the spheres were classified in that category in the experimental results. Quantitative results are given in Appendix D.

E. Discussion

Our results, as compared to DTS's ones, provide evidence of independence of the properties of isotropically equilibrated samples of rigid, frictionless spherical beads, on the dynamics in the assembling stage, if the compression is fast enough. Such final states can thus be regarded as an ideal model of random close packing (RCP) states. The RCP concept was criticized by Torquato *et al.* [10] as ill-defined, and these authors proposed to define a "most random jammed state" instead, as the one minimizing some order parameter among the variety of possible "jammed states" (*i.e.*, as we showed, stable mechanical equilibrium states). This is also the point of view of the DTS paper, emanating from the same group of authors, which we have been referring to. Our point of view here is more practical: we investigate the states that are likely to be obtained in an experiment (assuming friction mobilization can be entirely avoided). This is finally equivalent to the concept advocated by OSLN: if some "maximum randomness" is to be attributed to the RCP states, it is associated with the entropy of initial, low density configurations. What matters in practice is the volume occupied in initial configuration space by the set of particle arrangements that, after the compaction procedure has been applied, produce given global (statistical) properties. That different compaction algorithms lead to identical statistical properties of the final packings of rigid, frictionless beads might simply be explained [31], by the "basin of attraction" of such states for a wide class of compaction dynamics (all remaining strongly constrained by the impenetrability condition) comprising an overwhelming majority of configurations of the initial "granular gas" at lower density. The quantitative agreement between our results and those of DTS, which we have checked for force and interstice distributions, can be regarded as especially strong numerical evidence for such a uniqueness in RCP state properties, because ideal equilibrated packings of rigid, frictionless spheres are approximated by quite different routes. In the discussion between both groups (see the comment on the OSLN paper by the DTS group [80] and the reply by OSLN [81]), we therefore rather agree with OSLN. We insist however that all numerical results are in very good agreement, that the results obtained by DTS with *rigid* particles (with the connections between the equation of state of the hard sphere fluid, the distribution of contact forces and the geometry of the available, shrinking part of configuration space close to a volume minimum) are very accurate, valuable and interesting, and that part of the controversy is only apparent. In particular, definitions of *jammed states*, by the impossibility of particle motion abiding by steric exclusion without volume increase for DTS, and by the positive-definiteness of the stiffness matrix for OSLN, are exactly equivalent in the limit of rigid grains and coincide with the classical concept of a stable equilibrium state. Displacements minimizing (25) approach those that simply minimize the potential energy associated with external pressure in the rigid limit. In fact, we do not actually see why the relatively new term *jamming* should be necessary in that case, and we therefore avoid it.

Another conclusion is that standard MD methods compare well with specifically designed methods that deal with rigid particles, and prove able to approach the rigid limit with satisfactory, if admittedly smaller, accuracy. Recalling that $\kappa = 39000$ corresponds to glass beads under 10 kPa, it seems that laboratory samples under usual conditions might in principle (if friction mobilization can be suppressed) approach the ideal (rigid particle) RCP state.

The isotropic packing state is modified and apparently evolves towards gradual crystallization as longer stages of agitation are allowed at lower density in the assembling process, as witnessed by the small, but systematic differences between A and A' configurations (precisely how and to what extent final packings are affected depending

State	d_c/a	Z	Z_{cr}	Q_6	$Q_6^{\rm loc}$	$Q_6^{\rm loc,cr}$	x_{cr}	$\langle n_{cr}\rangle$
A	1.35	12.36 ± 0.03	2.91 ± 0.06	$(1.7 \pm 0.3) \times 10^{-2}$	0.392 ± 0.001	0.417 ± 0.003	0.080 ± 0.005	19.8
A'	1.35	12.50 ± 0.02	3.13 ± 0.11	$(1.9 \pm 0.5) \times 10^{-2}$	0.398 ± 0.0005	0.420 ± 0.002	0.104 ± 0.006	54.8
A	1.40	13.11 ± 0.02	2.94 ± 0.06	$(1.6 \pm 0.3) \times 10^{-2}$	0.370 ± 0.001	0.394 ± 0.002	0.083 ± 0.006	22.8
A'	1.40	13.20 ± 0.02	3.16 ± 0.11	$(1.8 \pm 0.3) \times 10^{-2}$	0.377 ± 0.0006	0.397 ± 0.003	0.103 ± 0.006	64.5

TABLE II: Indicators of possible incipient crystalline order in states A and A' at $\kappa = 39000$. Z is the coordination number of first heighbors, Z_{cr} the "crystalline bond" coordination number, Q_6 and $Q_6^{\rm loc}$ the global and (average) local order parameters, $Q_6^{\rm loc,cr}$ its average value within crystalline regions, x_{cr} the fraction of "crystalline" particles and $\langle n_{cr}\rangle$ the mass average of the number of particles in a "crystalline cluster". First neighbors are defined here as those closer than distance $d_c = 1.35a$ or $d_c = 1.40a$, near the first minimum in $g(r)$.

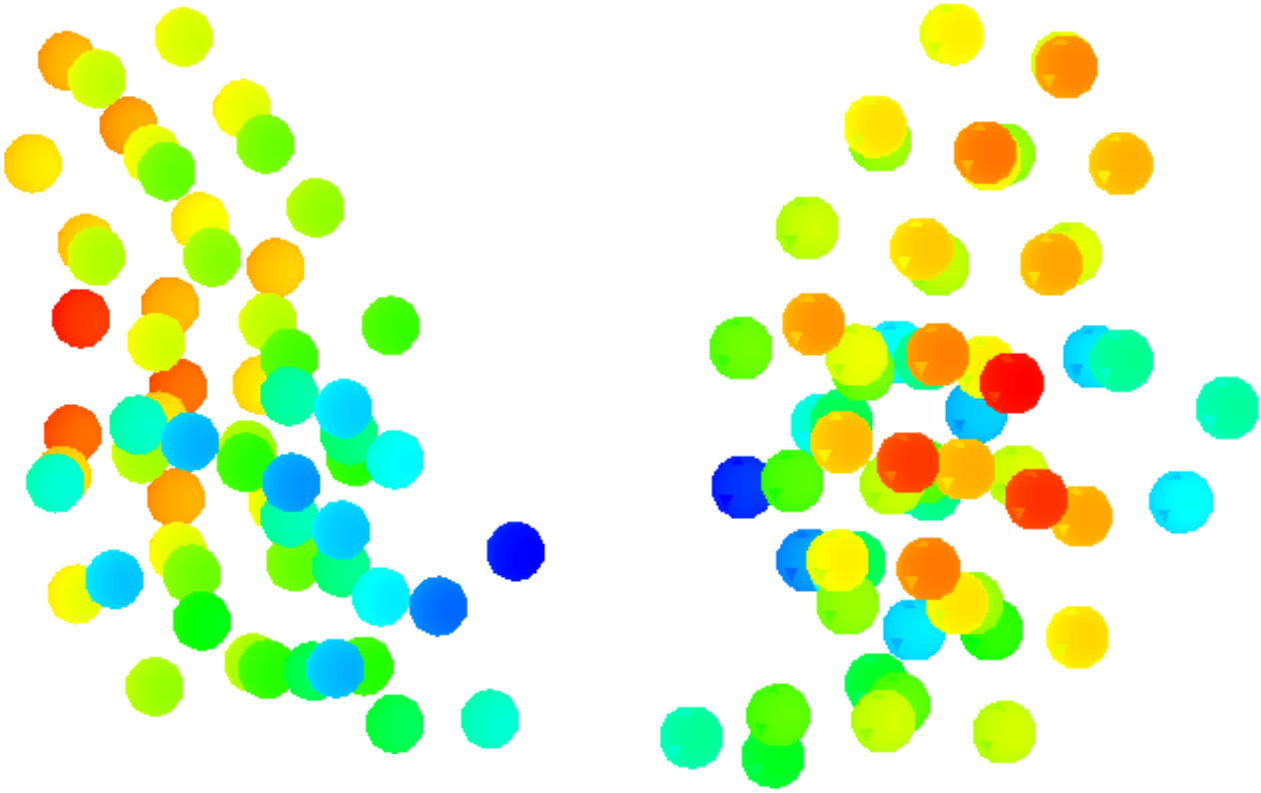

FIG. 7: (Color online). Arrangement of particles within one "crystalline cluster", seen from two different angles. Sphere radii are divided by two to visualize center positions better, and colors correspond to coordinates along one axis.

on compaction history is beyond the scope of this paper). An appropriate practical definition of random close packing can therefore, according to our observations, be proposed as *the (apparently unique) state obtained on equilibrating rigid, frictionless spheres under isotropic pressure in the limit of fast compaction processes*. As noticed, in particular, by OSLN, the RCP state has various remarkable properties and many variables can be expressed with power laws of the distance to rigidity threshold (in terms of density). We saw here that some of those results are direct consequences of the isostaticity property (in particular the relation between pressure and density, or bulk modulus and pressure, and the density dependence of the shape of the contact peak in the pair correlation function). In the following we explore to what extent packings made with friction resemble that ideal RCP state, and systems that are more than barely rigid share some of the properties observed in that section.

Anisotropic packings of rigid, frictionless balls, under other confining stresses than a hydrostatic pressure, should differ from this RCP state. Numerical simulations of gravity deposited packings of frictionless beads might produce different states from the one studied here (numerical results of refs. [24, 25] could be analysed in this respect).

IV. LOW-PRESSURE STATES OF FRICTIONAL PACKINGS OBTAINED BY DIFFERENT PROCEDURES

We now turn our attention to looser states (Section IV A) as well as dense ones (Section IV B) obtained with frictional grains, and discuss some of their geometric properties (Section IV C) and some features of their contact networks (Section IV D). Section IV E investigates, as a special, theoretical limit, the case of an infinite friction coefficient. Section IV F discusses our results with reference to other numerical and experimental studies.

A. Frictional packings assembled by direct compression

It is well known that the introduction of friction in granular packings tends in general to reduce density and coordination number, as observed in many recent numerical simulations (see *e.g.* [24, 25, 26, 27]), and that frictional granular assemblies, unlike frictionless ones, can be prepared in quite a large variety of different states. In the field of soil mechanics, sand samples are traditionnally classified by their density [11], which determines behaviors that have been observed in simulations of model systems as well, although fabric (or distribution of contact orientation) is also recognized as an important state variable [19, 21, 27]. Moreover, for a given assembling process, the resulting packing properties were observed numerically to depend on the level of viscous dissipation in contacts (parameter ζ) [24, 25]. This loss of uniqueness renders the definition of *random loose packing*, supposed to be the state of least density able to resist externally applied stresses, much more problematic that the random close packing discussed in the previous section. Such a state should at least depend on the friction coefficient, but might also differ according to the assembling method, each one producing a minimum density for a given choice of its control parameters. One definition thus involves slow sedimentation in a fluid, with the lowest density obtained in the limit when buoyancy forces nearly compensate the weight of the grains [82]. Engineering studies on sands usually resort to a conventional definition of minimum density, based on standardized procedures [83].

In the present study we chose to bypass the painstaking computations needed to mimic actual laboratory assembling methods, and to explore rather plausible microstructures obtained, for one given value of the friction coefficient ($\mu = 0.3$) by different numerical procedures that produce homogeneous and isotropic periodic samples. One issue, in particular, is whether samples made in the laboratory with the RCP density resemble the ones studied in Section III.

1. *Looser packings assembled with final friction coefficient*

We used direct compression of a granular gas in the presence of friction ($\mu = 0.3$), another standard numerical procedure [26, 27, 28], in which the obtained density and coordination number are decreasing functions of the coefficient of friction [24, 25, 26, 27], to produce rather loose samples hereafter referred to as D (B and C ones, to be defined further, denoting denser ones, closer to A, but arguably more "realistic"). D samples were made with exactly the same method as A ones, except that the friction coefficient $\mu = 0.3$ was used instead of $\mu = 0$. In principle, D configurations should depend on initial compaction dynamics: increasing I could produce denser equilibrated packings, just like a larger height of free fall, whence a larger initial kinetic energy, increases the density of configurations obtained by rain deposition under gravity [71]. With our choice of parameters, $I \leq 10^{-3}$ and $\zeta = 0.98$, we obtain solid fractions $\Phi = 0.5923 \pm 0.0006$ and coordination numbers $z^* = 4.546 \pm 0.009$, once the population of rattlers, which amount to a fraction $x_0 = (11.1 \pm 0.4)\%$ of the total number of grains, is excluded from the count. These data correspond to $P = 1$ kPa (or $\kappa \simeq 181000$). Very similar results are obtained on using a different, but low enough pressure, such as 10 or even 100 kPa, as remarked in [49] (where 2D samples were assembled by oedometric compression), and as indicated in table III, while the quasistatic compression from $P = 1$ kPa would produce different states at the same pressure. The influence of ζ should of course gradually disappear on imposing smaller values of the reduced compression rate I. As reported in table III, a value of the damping parameter ten times as small as the standard one $\zeta = 0.98$ results in quite similar configuration properties, on compressing a loose granular gas under $P = 10$ kPa, with $I \leq 10^{-3}$. So did in fact faster compressions, with I reaching 0.1, keeping $\zeta = 0.98$. A practical definition of a (μ-dependent) limit of loose packing obtained by direct compression, with presumably no influence of ζ, could be attempted as the limit $I \to 0$. We did not strive to approach it any further than the D states with the parameters listed above and condition $I \leq 10^{-3}$, the results of table III suggesting that our choices nearly achieved independence on dynamical parameters.

Looser arrangements of equal-sized spherical particles can be stabilized with adhesive contact forces, *e.g.* on introducing the capillary attractions produced by the menisci formed by a wetting fluid in the interstices between neighboring grains [84].

In addition to packing fraction Φ, coordination number z^*, fraction of rattlers x_0, table III lists the reduced second moment $Z(2)$ of the normal force distribution, as defined in (27), the proportion of 2-coordinated beads (to be discussed in Section IV D), x_2, and the average values of ratios $||\mathbf{T}||/N$ among contacts carrying normal forces larger and smaller than the average, respectively denoted as M_1 and M_2. As a result of some amount of quasistatic

TABLE III: Isotropic states of type D, from direct compression of the granular gas at the indicated pressure (rows marked "gas"), or from gradual, quasistatic compression (rows marked "QS") of solid samples made at the lowest pressure 1 kPa (or $\kappa \simeq 181000$). Tests of the influence of viscous dissipation parameter ζ and maximum value $I_{\max}$ of reduced strain rate in compression are also made for configurations compressed from a granular gas to 10 kPa.

Origin	P (kPa)	ζ	$I_{\max}$	Φ	z^*	x_0 (%)	x_2 (%)	$Z(2)$	M_1	M_2
gas	1	0.98	10^{-3}	0.5930 ± 0.0007	4.546 ± 0.009	11.1 ± 0.4	2.39	1.58	0.160	0.217
gas	10	0.98	10^{-3}	0.5946 ± 0.0006	4.59 ± 0.02	10.2 ± 0.2	2.07	1.59	0.159	0.213
gas	10	0.098	10^{-3}	0.5938 ± 0.0008	4.61 ± 0.02	10.9 ± 0.2	1.79	1.57	0.150	0.194
gas	10	0.98	10^{-1}	0.5931 ± 0.0002	4.60 ± 0.01	10.2 ± 0.7	1.80	1.59	0.159	0.212
QS	10	0.98	10^{-3}	0.5931 ± 0.0006	4.641 ± 0.011	10.1 ± 0.4	2.33	1.46	0.146	0.188
gas	100	0.98	10^{-3}	0.5975 ± 0.001	4.69 ± 0.02	8.9 ± 0.5	1.66	1.61	0.153	0.197
QS	100	0.98	10^{-3}	0.5936 ± 0.0006	4.79 ± 0.02	8.6 ± 0.4	2.05	1.40	0.138	0.178

compression of the initial assembly, the width of the force distribution decreases, as witnessed by smaller values of $Z(2)$ in table III, and so does the mobilization of friction, as measured by M_1 and M_2. The effects of compression on the structure and the forces are further studied in paper II [37]. On comparing numerically simulated loose packings to experiments, it should be recalled that samples are assembled under low pressures in the laboratory: the hydrostatic pressure under a 1 cm thick layer of glass beads is about 0.15 kPa. Numerical configurations under higher confining pressures corresponding to mechanical tests in the laboratory (*e.g.*, sound propagation) are more appropriate models if the testing pressure is significantly larger than the initial, assembling pressure – as for the "QS" samples of table III.

The effects of such proportions of rattlers in granular packings as reported in table III have to our knowledge never been studied in detail. It should be emphasized that this relatively large population of rattlers does not jeopardize the global stability of equilibrium configurations, as the stiffness matrix of the force-carrying network was found devoid of floppy modes (apart from harmless, localized ones associated with 2-coordinated particles, to be discussed in Section IV D). On mixing several populations of grains with different diameters, it is expected that for some proportions in the mixture one or several classes of grains will carry most of the forces, while the others will comprise many rattlers. This idea of a "dominant" or force-carrying class in a mixture is at the basis of a semi-empirical approach to a maximum packing fraction concept in granular mixtures, which is used in concrete mixture proportioning [85]. The existence of more than 10% rattlers in monodisperse systems is perhaps less intuitive, but should be taken into account if one attempts an accurate prediction of macroscopic behavior from micromechanics.

2. *Use of low, non-vanishing friction coefficients*

As recalled in Section III A, one achieves maximum densities on equilibrating frictionless packings under an isotropic pressure. Compaction strategies can therefore be regarded as procedures designed to circumvent the influence of friction. One possibility is to lubricate the grains, as in the experimental study reported in [86], in which Jia and Mills prepared bead packings in the presence of a lubricant. If all intergranular friction could be suppressed in the assembling procedure, then the structure of isotropic packings would be the one denoted as A, studied in Section III. It is worth investigating, though, the influence of a small value of the friction coefficient, as setting $\mu = 0$ exactly is practically impossible. We therefore made samples, denoted as B, by compressing a granular gas, just like in the A and D cases, but with $\mu = 0.02$. This can be regarded as a rough model for imperfectly lubricated grains (in paper III we compare our results on elastic properties of B samples to the experimental ones obtained by Jia and Mills [86]). On limiting inertia parameter I to small values in the assembling stage ($I < 10^{-4}$), we observed that this small friction coefficient had a notable effect on the final solid fraction under $P = 1$ kPa ($\kappa \simeq 181000$), $\Phi = 0.627 \pm 2.10^{-4}$, while the coordination number on the active structure was slightly reduced compared to the frictionless (A) case, down to $z^* = 5.75 \pm 8.10^{-3}$, and the fraction of rattlers raised slightly, to $x_0 = (1.95 \pm 0.02)\%$.

B. Dense, frictional packings obtained by shaking

Another practical strategy to obtain dense configurations is to shake, vibrate or apply repeated "taps" on granular samples [5, 35, 36]. Such procedures involve the introduction of kinetic energy into already quite dense assemblies. In order to investigate their possible effects at a limited computational cost, we avoided the direct simulation of repeated shakes and adopted the following procedure. Starting from the dense A configurations (made without friction and described in Section III), we first applied a homogeneous expansion, multiplying all coordinates by a common factor λ slightly larger than 1. With equilibrated A states under confinement level $\kappa = 39000$, the chosen value $\lambda = 1.005$ is more than enough to separate all pairs in contact. Then, in order to mimic, in an idealized way, the motion set up by a

shaking excitation, the beads are given random velocities (chosen according to a Maxwell distribution), and interact in collisions which preserve kinetic energy, while the volume of the cell is kept constant. This "mixing" stage is simulated with the "hard sphere molecular dynamics" (event-driven) scheme (just like our initial granular fluids are prepared at $\Phi = 0.45$, as described at the beginning of Section III). It is pursued until each particle has had $n_{\rm coll} = 50$ collisions on average. The final preparation stage is a fast compression: velocities are set to zero, particles regain their elastic and dissipative properties (as defined in Section II A, with friction coefficient $\mu = 0.3$, and viscous dissipation, $\zeta = 0.98$), the external pressure $P = 10$ kPa is applied *via* the deformable periodic cell, until a final equilibrium is reached.

The final state is hereafter referred to as C. Quite unsurprisingly, its solid fraction, $\Phi = 0.635 \pm 0.002$, stays very close to the RCP value obtained in the A state. However, the coordination number is considerably lower, $z^* = 4.56 \pm 0.03$, very close to the value obtained in the loose ($\Phi \simeq 0.593$) D state, while the proportion of rattlers raises to $x_0 = (13.3 \pm 0.5)\%$. Remarkably, on comparing states B and C, the latter has a higher density, but a much lower coordination number, and a much higher fraction of rattlers. Table IV gathers some of the parameters characterizing the four different packing states studied throughout the following of the present paper. (M_1 and M_2 were defined in connection with table III). From table IV, configurations with low coordination numbers (C and D) appear to exhibit a somewhat wider normal force distribution (as measured by $Z(2)$), and a significant mobilization of friction, with typical values of $||\mathbf{T}||/N$ around $\mu/2 = 0.15$ for larger than average normal force components N (M_1), and significantly above $\mu/2$ for smaller N values (M_2).

We did not thoroughly investigate the influence of parameters λ and $n_{\rm coll}$, introduced in the preparation procedure, on the resulting C states. In the following we focus on configurations obtained with the values $\lambda = 1.005$ and $n_{\rm coll} = 50$. Yet, we noted that an increase of λ to 1.01 entailed only very slight changes of Φ and z^* (which respectively decreased to 0.633 and 4.54), and that the suppression of the "mixing" stage (*i.e.*, setting $n_{\rm coll}$ to zero) resulted in much higher z^* values (around 5.5).

The existence of C states shows that there is no systematic relationship between density and coordination number, in spite of some statements in the literature [7]. Of course, for one particular assembling method both quantities are expected to vary in the same direction as functions of a control parameter. For instance, on preparing samples by deposition under gravity, both density and coordination number are increasing functions of the height of free fall [71]. However, our results show that different preparation methods might lead to contrasting results. It remains to be determined whether experimental packings of spherical grains, with solid fraction in the 0.635 to 0.64 range, have coordination numbers close to 6 like our numerical A state, or close to 4.5 like our numerical C state, the answer depending on how such samples were assembled.

C. Geometric characterization

As observed in previous experimental [7] and numerical [24] results, pair correlation functions present the same features at lower densities as at the largest one $\Phi \simeq 0.64$, in a weakened form, as shown on Fig. 8. On

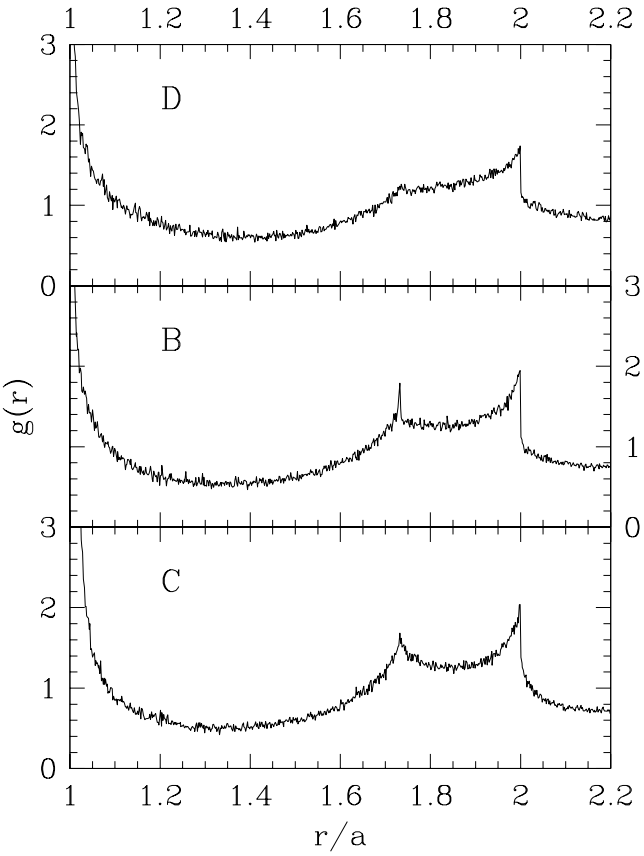

FIG. 8: Pair correlation functions $g(r)$ (definitions $g^I(r)$ and $g^{II}(r)$ coincide on this scale) for configurations B, C, D.

comparing those functions for states A to D, we observed what follows.

- C samples, obtained from A ones after small rearrangements, exhibit pair correlations that only differ in the detailed shape of the peaks (*e.g.* below $1.05a$), and is indistinguishable elsewhere.
- In spite of the large number of rattlers in samples C and D, $g^I(r)$ and $g^{II}(r)$ (as defined in Section III C) cannot be distinguished on the scale of Fig. 8.
- The depth of the trough between $r/a = 1.1$ and $r/a = 1.5$ increases with density.
- The integral below the peaks correlates with density, but the height and sharpness of the *drop* at

TABLE IV: Isotropic states ($\kappa \simeq 39000$ for A and C, $\kappa \simeq 181000$ for B and D) for different assembling procedures.

Procedure	Φ	z^*	x_0 (%)	x_2 (%)	Z(2)	M_1	M_2
A	0.6370 ± 0.0002	6.074 ± 0.0015	1.3 ± 0.2	0	1.53	0	0
B ($\mu_0 = 0.02$)	0.6271 ± 0.0002	5.80 ± 0.007	1.95 ± 0.02	$\sim 10^{-4}$	1.52	0.016	0.018
C ($\lambda = 1.005$)	0.635 ± 0.002	4.56 ± 0.03	13.3 ± 0.5	2.64	1.65	0.135	0.181
D	0.5923 ± 0.0006	4.546 ± 0.009	11.1 ± 0.4	2.39	1.58	0.160	0.217

$r/a = \sqrt{3}$ and $r/a = 2$ correlate with coordination number (which is larger for B than for C), in agreement with the interpretation of such features suggested in Sec. III D.

The cumulated distribution of interstices, or near neighbor coordination number $z(h)$, is shown on Fig. 9 for samples A to D. Fig. 9 shows that, as expected, $z(h)$ cor-

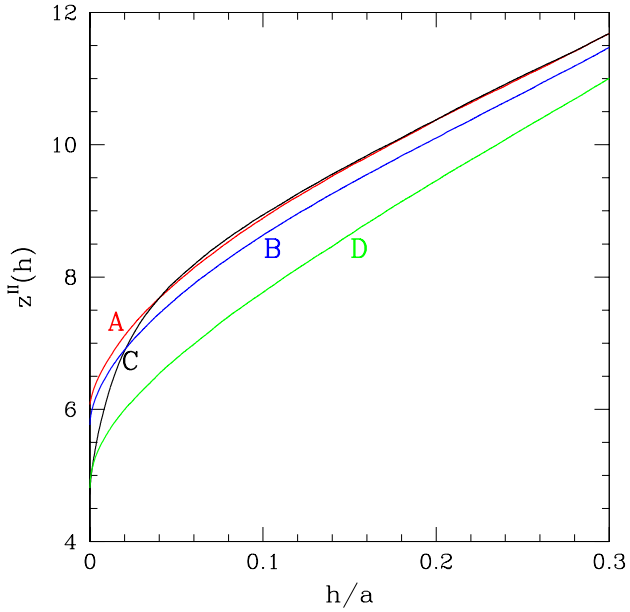

FIG. 9: (Color online) Coordination number for neighbors at distance $\leq h$, $z^{II}(h)$, for configurations A (red), B (blue), C (black) and D (green).

relates with coordination number for small h and with density for larger distances, $h \geq 0.04a$. We preferably use definition $z^{II}(h)$, which is obtained on bringing the rattlers in contact with the backbone with small, random forces, as explained in Sec. III C. $z^{II}(h)$ can be thought of as more physically meaningful than $z^I(h)$, which directly results from the simulation of the packing, and is somewhat ambiguously defined because the positions of the rattlers are not specified. ($z^{III}(h)$, which is obtained on discarding rattlers altogether, involves a mutilation of the packing geometry). $z^I(h)$ and $z^{II}(h)$ might be fitted by power laws:

$$\begin{aligned} z^I(h) &= z^I(0) + A_I h^{\beta_I} \\ z^{II}(h) &= z^{II}(0) + A_{II} h^{\beta_{II}} \end{aligned} \qquad (35)$$

In (35), $z^{II}(0)$ is the *geometric* coordination number once all rattlers are pushed against the backbone. It is larger than the *mechanical* coordination number, which is simply denoted as z. Specifically, because all rattlers, on pushing them against the backbone, are dealt with as frictionless, one has:

$$z^{II}(0) = z + 6x_0 - \frac{2N_{rr}}{n}, \qquad (36)$$

in which N_{rr} is the final number of contacts between rattlers once they are positioned against the backbone. One has $z^I(0) \simeq z$ as a very good approximation, since contacts carrying no force in the equilibrated state obtained by MD are very scarce. Figs 10, 11 and 12 display $z^I(h) - z$ and $z^{II}(h) - z^{II}(0)$ as functions of h on logarithmic plots for samples D, B and C. These figures (on

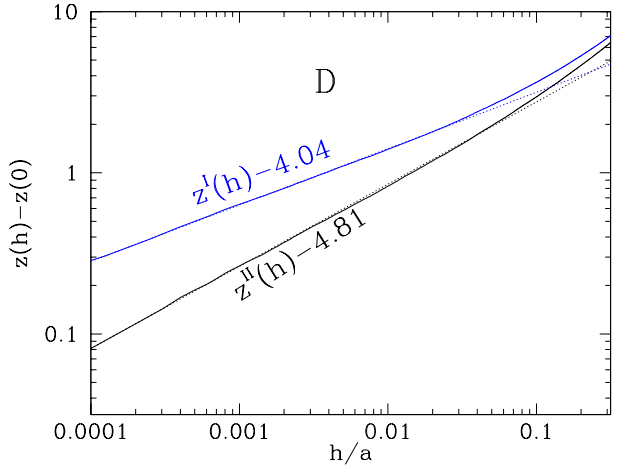

FIG. 10: (Color online) $z^I(h) - z$ (black) and $z^{II}(h) - z^{II}(0)$ (blue) versus h on doubly logarithmic plot for D samples at lowest pressure. The slopes of the corresponding dotted straight lines (power law fits) are $\beta_{II} = 0.51$ and $\beta_I = 0.35$ (see Eqn. 35).

which the corresponding values of $z \simeq z^I(0)$ and $z^{II}(0)$ are also provided) show that z^I and z^{II} have quite different h dependences, which should be accounted for on studying the closing of contacts due to compression, as we shall see in paper II [37]. As a result of the computation leading to the equilibrated state, many pairs of neighbors end up separated by a very small interstice, so that $z^I - z$ already reaches values larger than 0.3 for $h = 10^{-4}a$ in samples C and D. z^I then grows with h

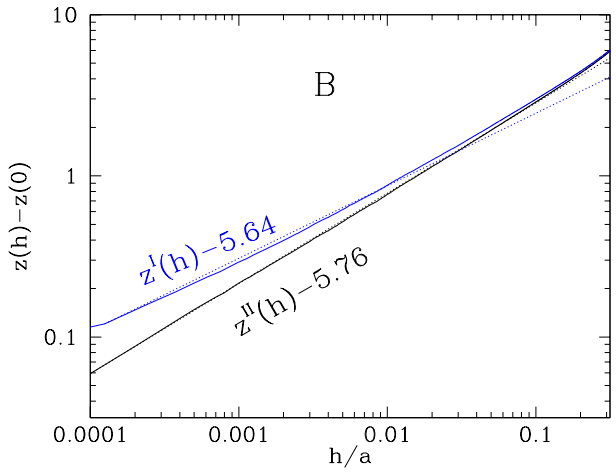

FIG. 11: (Color online) Same as Fig. 10, for B samples. Dotted lines have slopes $\beta_{II} = 0.56$ and $\beta_I = 0.45$.

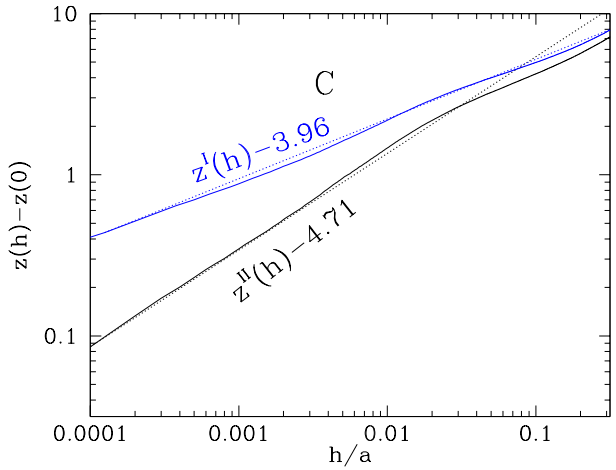

FIG. 12: (Color online) Same as Fig. 10, for C samples. Slopes of dotted straight lines: $\beta_{II} = 0.6$ and $\beta_I = 0.37$.

more slowly than z^{II}, with $\beta_{II} > \beta_I$, and a power law fit of lesser quality. Exponent β_{II}, which should be regarded as a more intrinsic quantity than β_I, appears to correlate with solid fraction. It has the same value 0.6 in samples C and A (Figs 12 and 6), decreases to 0.55 in the intermediate density state B, and to 0.51 for the least dense one, D. The power-law form of z^{II} extends to $h \simeq 0.3$ in configuration A, to about $h \simeq 0.2$ in configuration B, and only to 0.04 and 0.05 for C and D. Those latter small values preclude comparisons with the experimental data of [7]. For h values smaller than 10^{-4}, the lowest limit on the axis on Figs. 10, 12 and 11, the gap h is of the same order as elastic deflections, κ^{-1}, and we do not observe simple power laws, just like in the situation represented on Fig. 6(b).

All indicators of incipient crystalline order given in table II for frictionless A samples take lower values in states B and D, while C configurations, due to their geometric proximity, are close to A ones in this respect. Already very scant in dense configurations assembled without friction, traces of crystallization are thus totally negligible in looser ones obtained with frictional beads. Like for A samples, numerical data on configurations around one sphere i, as characterized by the pair $(\hat{Q}_4(i), \hat{Q}_6(i))$, used by Aste *et al.* [7], are presented for states B, C, and D and compared to their experimental results in Appendix D.

D. Properties of contact networks

We now turn our attention to the properties of the force-carrying structure. The distribution of local coordinations is given in table V, for both mechanical (I) and geometric (II) definitions of contacts, for states B to D. Compared to the A case (table I), the distribution is shifted to lower values, with 4 and 5 the most frequent ones (rather than 6) in low coordinated packings C and D. Those samples also have quite a large population of 3-coordinated spheres, and a notable one of divalent (2-coordinated) particles. This contrasts with the frictionless case for which $x_2 = x_3 = 0$. Without friction, divalent spheres, from Eqn. 20, written with $N_c = 2$, $N_f = 3$, $h = 0$, would imply a mechanism and therefore an instability, and 3-coordinated ones, in the absence of external forces and cohesion, cannot be equilibrated by non-vanishing normal forces the net effect of which necessarily pushes them away from the plane defined by the 3 centers of their touching neighbors (the non-generic case with the four sphere centers within the same plane leading to an instability). This is schematized on fig. 13. Spheres with three contacts therefore need some mobilization of friction to transmit non-vanishing forces in an equilibrium configuration, for tangential components are requested to cancel this net repulsion. The Coulomb condition then restricts such possible configurations to flat enough tetrahedra $(ABCO)$ for contact forces to remain within the friction cone. This explains the small value of x_3 in low friction ($\mu = 0.02$) B samples.

State	x_0	x_1	x_2	x_3	x_4	x_5	x_6	x_7	x_8	x_9	x_{10}
B (I)	1.95	0	0.05	0.5	16.3	26.9	27.5	18.4	7.1	1.4	0.1
C (I)	13.3	0	2.6	15.1	26.5	23.4	13.2	4.8	0.9	0.15	0
D (I)	11.1	0	2.4	13.8	29.1	25.6	13.3	4.0	0.7	0.03	0
B (II)	0	0	0	2.1	15.3	26.5	27.5	18.9	7.8	1.6	0.2
C (II)	0	0	0	18.9	22.8	27.0	18.6	9.3	2.8	0.5	0.1
D (II)	0	0	0	17.2	25.4	29.0	18.5	7.7	1.9	0.3	0

TABLE V: Percentage x_i of grains having i contacts in configurations B, C and D, on ignoring contacts with or between rattlers (I), or on fixing them onto the backbone with small, random forces (II).

With friction, the small structure formed by one sphere having 2 contacts with fixed objects (Fig. 14), due to Eqn. 19, in which the number of degres of freedom (6)

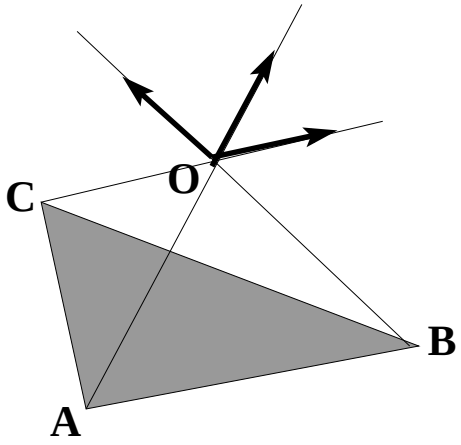

FIG. 13: If one sphere, centered in point O, is in contact with three others, with centers in A, B and C, then normal components of the contact forces (drawn vectors), carried by the respective lines of centers AO, BO and CO, necessarily push the sphere in O away from the plane defined by triangle ABC.

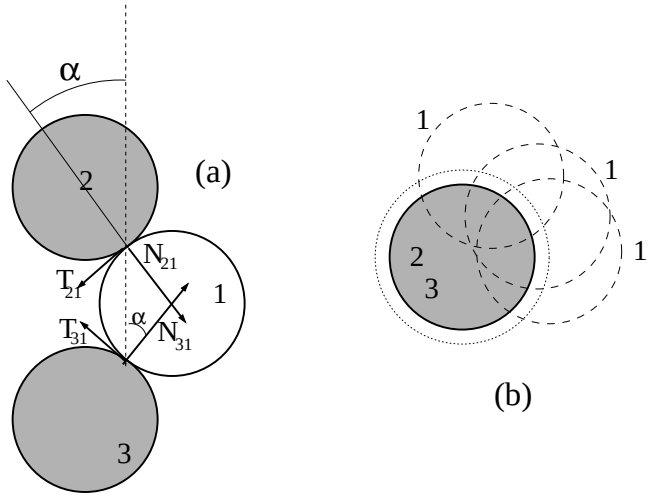

FIG. 14: Equilibrium and free motion (mechanism) of one sphere (marked 1) with two contacts (with particles marked 2 and 3). (a): in the plane of the three centers, normal and tangential components of the two contact forces balance along the line joining the contact points (dotted line). (b): seen from above, along the direction of the line of the centers of spheres 2 and 3, sphere 1 can move and occupy the different positions depicted with dashed lines, its center describing the dotted circle around the 2-3 axis.

is equal to the number of contact force coordinates, has a degree of force indeterminacy equal to its number of independent mechanisms: $\mathrm{H} = k$. In fact, both numbers are equal to 1. Self-balanced contact forces (see first part of Fig. 14) are oriented along the line joining the two contacts, just like in the corresponding 2D case dealt with in [47], and their amplitude is a free parameter (the degree of "wedging" of the grain in the corner formed by its two neighbors [47]). Such a possibility requires in practice that the angle, which we denote as α (Fig. 14), between the line joining the centers of 1 and 2 and the one joining the contact points be smaller than the angle of friction, for the total contact force to stay within the Coulomb cone. In C and D samples, we observed $\tan\alpha$ to be distributed rather evenly between 0 and μ, while the intensity of forces transmitted by divalent spheres ranged from 0 to a few times Pa^2.

The mechanism associated with divalent spheres is a free rolling motion on the two contacts, the line joining the contact points being the instantaneous axis of rotation, as shown on fig. 14(b). In this motion, it is readily checked that the rules given in Appendix B for the evolution of contact forces in the case of rolling and pivoting specify that contact forces will remain carried by the line joining the two contacts, with a constant intensity, as such contacts move on the surface of the fixed spheres. Such forces will do no work and the kinetic energy of the mobile sphere as well as the elastic energy stored in its two contacts will be kept constant. The equilibrium of the divalent particle is thus marginally stable, with matrix $\underline{\underline{\mathbf{K}}}^{(2)}$ causing zero acceleration to the free motion. However, such a motion does affect the balance of *moments* on spheres marked 2 and 3 on fig. 14, since the constant forces are applied at different points on their surfaces. Therefore the stability of such free motions, as regards the global contact network, requires some additional analysis – which is tackled in Appendix E, where it is concluded that the packing remains stable. Unlike in frictionless packings [32, 87], mechanisms in the presence of friction do not necessarily lead to instabilities. On building the constitutive stiffness matrix $\underline{\underline{\mathbf{K}}}^{(1)}$ in the samples we studied, we could check that no other mechanism was present on the backbone than those rolling motions of divalent spheres. Once some stiffness element is introduced to impede the free motion of divalent spheres, one can *e.g.* check that the Cholesky factorization of the stiffness matrix only involves strictly positive terms on the diagonal. These free motions were attributed some energy cost, such alteration of the matrix having no effect on the response to externally applied stress increments. There can be no contact between two divalent spheres, as the equilibrium of the pair, each one with two forces carried by the line joining its two contact points, as on Fig. 14, is impossible.

On the backbone, with $n(1-x_0)$ spheres and $N_f = 6n(1-x_0)+3$ degrees of freedom, one has on average $z^*n(1-x_0)/2$ contacts and $k = 3 + x_2 n$ independent mechanisms, hence a degree of force indeterminacy (hyperstaticity), from (19), given by:

$$\begin{aligned} \mathrm{H} &= N_f^* \frac{z^* - z_0^*}{4} = N_f^* \frac{z^{**} - 4}{4}, \text{ with} \\ N_f^* &= 6n(1-x_0), \\ z_0^* &= 4 - \frac{2x_2}{3(1-x_0)} \text{ and} \\ z^{**} &= z^* + \frac{2x_2}{3(1-x_0)} \end{aligned} \tag{37}$$

The backbone has N_f^* degrees of freedom and is devoid of force indeterminacy ($\mathrm{H} = 0$) when its coordination number is equal to z_0^*. Because of the mechanisms associated with divalent beads z_0^* is strictly smaller than 4. Alternatively, one can define a "corrected" backbone coordination number z^{**}, as written in (37), which is equal to 4 in the absence of force indeterminacy. As to the global mechanical coordination number z_0 corresponding to the absence of force indeterminacy, its value, given by

$$z_0 = 4(1 - x_0) - \frac{2x_2}{3}, \tag{38}$$

is well below 4. From the data of table V, z_0 is about 3.45 in state C and 3.54 for D (while z is close to 4 and z^* exceeds 4.5). Although H is relatively small compared to the number of degrees of freedom N_f, the samples with friction and low coordination are still notably hyperstatic – a conclusion shared by other studies [24], which we reach here in the slightly different context of packings in a uniform state of stress. Unlike for frictionless sphere assemblies, there is actually no special reason to expect packings with intergranular friction to become isostatic in the rigid contact limit. This essential difference is that contact forces can no longer be regarded as enforcing hard geometric constraints like impenetrability, and hyperstatic configurations do not require exceptional arrangements or matching of particle sizes as in the frictionless case [32, 75, 77, 88]. The argument that isostaticity should naturally arise when some flow is arrested or when a "fragile" solid-like particle assembly is on the verge of an instability leading to motion, as suggested, *e.g.*, in [89], ignores the possibility for granular packings to have both floppiness (non-trivial mechanisms, $k > k_0$ in Eqn. 19) and some force indeterminacy (self-balanced sets of contact forces, $\mathrm{H} > 0$ in Eqn. 19), a simple example thereof being the divalent sphere of Fig. 14. A non-vanishing degree of hyperstaticity whatever the stiffness level κ enables changes in the shape of the force distribution in response to a pressure increase, as will be studied in paper II [37]. The force distribution is no longer a geometrically determined quantity,

The distribution of normal components of contact forces (normalized by its average $\langle N \rangle$) is shown on Fig. 15 for all 4 configurations A, B, C, and D, at the lowest pressure (as given in Table IV), right at the end of the assembling process. We observe, as in many other numerical [25, 73, 90, 91] and experimental [92, 93] studies, an approximately exponential decay of $P(f)$ for large values, which is somewhat slower in states with low coordination number (in agreement with the values of $Z(2)$ given in table IV). It should be pointed out, however, that much larger differences between force distributions in the four studied configurations will appear on increasing the confining pressure (see [37], paper II), as already apparent in the dependence of $Z(2)$ on the previous history of D samples in table III.

All probability distribution functions show a local minimum for $f \to 0$, except in state C. Although it was

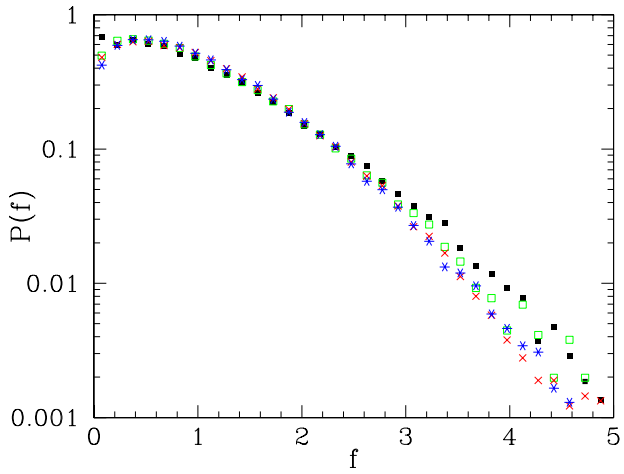

FIG. 15: (Color online) Distribution of normal forces, normalized by its average, $f = \frac{N}{\langle N \rangle}$, in states A (red crosses), B (blue asterisks), C (black square dots) and D (green open squares) at the lowest simulated pressure.

remarked in past publications [94] that an upturn of the p.d.f. at low forces, as for C configurations, appeared when packings were not fully equilibrated, C configurations satisfy equilibrium requirements as well as the others (with the criteria given at the beginning of Sec. III). As frictionless sphere packings are unstable for $z^* < 6$ [32], a certain level of friction mobilization is required in states B to D, even under isotropic stresses. In particular, non-vanishing tangential forces are indispensable to ensure the equilibrium of grains with 2 and 3 contacts, for which they relate to the local geometric configuration, as discussed above (see *e.g.,* Fig. 14). Some information about friction mobilization is given in Table VI. In Table VI we distinguish between contacts carrying normal forces larger and smaller than the average $\langle N \rangle$ (which is given by relation (22)). Those two populations of contacts, as first distinguished in [94, 95], as the "strong" and "weak" networks, are attributed different roles, especially under anisotropic stresses. We merely use these categories here to gather information, in a compact, summarized form, about some aspects of force networks, which correlate to the force level. Table VI shows that, although 3-coordinated particles tend to carry small forces on average, a notable proportion of them, and of the divalent ones, participate in the strong "force chains" with larger than average force levels. Friction mobilization is necessary in the contacts with such spheres, and reaches similar levels on average in the whole network. It it larger for contacts carrying small loads.

E. The limit of large friction coefficients

Motivated by the search for an isostatic limit in packings with intergranular frictions, Zhang and Makse [96] assembled numerical packings with friction coefficients

State	X_1	M_1	M_2	$N^{(2)}$	$X_1^{(2)}$	$M_1^{(2)}$	$M_2^{(2)}$	$N^{(3)}$	$X_1^{(3)}$	$M_1^{(3)}$	$M_2^{(3)}$
B	0.42	0.016	0.018	n. d.	n. d.	n. d.	n. d.	0.23	0.09	0.02	0.01
C	0.41	0.14	0.18	0.58	0.19	0.14	0.17	0.24	0.09	0.13	0.04
D	0.41	0.16	0.22	0.71	0.22	0.16	0.18	0.26	0.10	0.15	0.05

TABLE VI: For states B, C, and D, at the lowest pressure (see table IV), proportion X_1 of contacts carrying normal forces larger than the average $\langle N\rangle$, average ratio $\frac{||\mathbf{T}||}{N}$ for contacts with $N > \langle N\rangle$ (respectively, $N < \langle N\rangle$) M_1 (resp. M_2). The same quantities with superscripts (2) and (3) apply to contacts implying spheres of coordination 2 and 3. $N^{(2)}$, $N^{(3)}$ are the average normal forces carried by these two populations of contacts, normalized by Pa^2. Note that divalent grains are absent in state B, and the corresponding quantities are therefore not defined.

equal to infinity. Then they could get $z^* \simeq 4.15$. In order to investigate, in paper III [38] the elastic properties of tenuous contact networks, we also prepared a set of 5 configurations on compressing a granular gas under $P = 1$ kPa with $\mu = +\infty$ and condition $I \leq 0.001$. These states, herafter referred to as Z configurations, have solid fraction $\Phi = 0.5917 \pm 0.0008$, backbone coordination number $z^* = 4.068 \pm 0.006$, proportion of rattlers $x_0 = (18.4 \pm 0.5)\%$ and of divalent beads $x_2 = (6.8 \pm 0.5)\%$, and H is indeed small in that case, $\frac{\mathrm{H}}{N_f^*} \simeq 0.031$. It seems therefore very plausible that the degree of hyperstaticity vanishes in this case, in the rigid limit $\kappa \to +\infty$, for slowly assembled packs. In the light of this observation, the absence of such a limit for finite μ can be attributed to sliding friction destabilizing barely rigid structures, which collapse and tend to form contacts in excess over the isostatic count.

F. Discussion

In Section III E, we insisted on the remarkable apparent uniqueness (in the statistical sense) of the equilibrium state, under isotropic loads, of frictionless sphere packings in the rigid limit, provided the slow evolution towards crystallization has been avoided by a fast enough compression in the assembling stage. One obvious conclusion of the study of frictional packings reported here, even though it is restricted to isotropic systems, is the existence of a wide variety of possible states, which cannot be classified by their sole density, since variations of solid fraction and cordination number are largely independent. We observed that the influence of dynamical parameters (I and ζ) could be minimized for slow enough compressions, and, κ becoming irrelevant if it is large enough (as shown by table III), the equilibrium state appears to be determined by the friction coefficient and the history of the sample in its assembling stage. The latter might be summed up by the values of both density and kinetic energy as a function of time. Kinetic energy should be compared to the potential energy of confining forces, and in that respect the idealized procedure used to assemble configurations C represents the limit of very strong vibrations in a dense system. States A and B, on the other hand, can be regarded as idealizations of the result of the compression of lubricated grains.

Our results about density and coordination number can be likened to observations made before in numerical models of sphere packings obtained with geometric construction rules [97]. The simplest versions of such algorithms [98, 99], which mimic deposition under gravity, add particles one by one by dropping and rolling them in contact with one or two previously deposited particles, until they are fixed when they rely on three contacts. Those produce packings with $z = 6$. More refined versions thereof [97, 100], which are motivated, in the case of [100], by the experimental process of compaction caused by repeated shakes, involve different stages, in which similar dropping and rolling moves alternate or combine with vertical expansions and/or Monte-Carlo steps, so that the whole process implies collective rearrangements. The final configuration is analysed in terms of "bridges" or "arches" [101], which are defined as sets of particles the final stabilization of which is mutual and collective. In such arches, each grain relies on three others, but some pairs mutually rely, in part, on each other. Those "bridged structures" have much lower coordination numbers, down to about 4.5.

It is not clear, though, to what extent our configurations, which were obtained within a full mechanical model, compare to those that result from such approaches. As shown, *e.g.*, in [102], deposition algorithms based on geometrical rules are supposed to ensure local stability properties, but the resulting granular pilings might turn out to be globally unstable. Moreover, a description of our packings as a sequence of arches placed one after another, assuming it is conceivable, would seem to contradict their homogeneity and isotropy: it seems rather arbitrary, in isotropic packings, to regard some particles as "relying" on some others. Such a description was therefore not attempted.

In low coordination states, more than 10% of the beads are rattlers, and this leads to important differences in several possible definitions of coordination numbers, which we recall here. The *global mechanical* coordination number, denoted as z, is the average number of active, force-carrying contacts per grain (rattlers contributing zero). It enters formula (22) which conveniently relates the pressure to the average normal contact force. The *backbone* coordination number, denoted as z^*, relates to z and to the fraction of rattlers x_0 as $z = z^*(1 - x_0)$, and is convenient to evaluate the degree of force indeterminacy H

in equilibrated packings, as in (37). We did not observe H to vanish in the $\kappa \to \infty$ limit. Finally the *geometric* coordination number, $z^{II}(0)$ is best defined on fixing the rattlers to the backbone and should be used to compare packing geometries.

Our D samples should be compared with the simulations reported by Zhang and Makse [96], in which loose sphere packings were assembled by isotropic compression. Those authors observed, in some cases, lower packing fractions than D values, $\Phi \simeq 0.57$. Their numerical samples are assembled with a different method: they use a strain-controlled procedure, with a constant compression rate, and then relax the final state at constant volume. This approach often involves reaching very high pressure levels, several orders of magnitude as large as the final value, before samples finally stabilize (see Fig. 3 of Ref. [96]). Some dependence on compressing rate is reported. Once translated into the dimensionless parameter I we have been using here, strain rates used in [96], using the typical pressure value $P = 100$ kPa, range between $I = 0.1$ and $I = 100$. The slowest compression reported in [96] is therefore 100 times as fast as the upper limit for $\dot{\epsilon}$ we have been enforcing in this work. Viscous forces also differ between the present simulations and those of Ref. [96], in which "global damping" terms are used (*i.e.*, forces opposing the individual motion of particles, rather than relative motions). Differences in final states thus confirm the variety of possible equilibrated configurations of frictional beads and the influence of micromechanical parameters and assembling protocol. Unlike us, Zhang and Makse speculate that isostatic packings could be obtained in the limit of slow compressions. This is however due to a divergence of interpretation, rather than a contradiction in numerical results, since their minimum coordination numbers z^*, excluding rattlers, are similar to ours, $z^* \simeq 4.5$. Zhang and Makse could only approach configurations devoid of hyperstaticity on setting the friction coefficient to infinity. The degree of force indeterminacy per degree of freedom on the backbone is still equal, from (37), to 0.141 in D samples and 0.145 in C ones, and varies very little with compression rate in the range we explored, which extends to significantly smaller values than the ones used in [96], as stressed above. It is not obvious whether special experimental situations might occur in which real granular assemblies approach vanishing degrees of hyperstaticity.

Surprisingly, frictional packings retain some floppiness on the backbone once equilibrated under pressure, in the form of innocuous local motions of divalent spheres. Such spheres, moreover, occasionnally transmit large forces. One can indeed check for the possibility of such local configurations in a simple experiment, which is conveniently done with *e.g.* ping-pong balls. Holding spheres 1, 2 and 3 with one hand in the position shown on Fig. 14 *without touching sphere 1*, and maintaining axis 2–3 vertical to minimize the perturbations due to its weight, one can observe that particle 1 can stay in equilibrium. If gently pushed it will roll around the line of contact points as described on Fig. 14(b) with little dissipation. The stability issue is further investigated in Appendix E.

Rattlers, of course, should not exist in the presence of gravity, but, as argued in Sec. III C, should be pushed against the backbone grains by their weight. What we defined as "method II" to deal with rattlers should lead to geometric characterizations comparable to experimental observations under gravity. Visualizations of packing configurations with X-ray tomography are still unable to provide accurate measurements of functions $z(h)$ for small interstices h, due to both limited resolution and to the effects of the unavoidable polydispersity and lack of sphericity of the particles. In the experiments reported in [6, 7], Aste *et al.* measure density fields in sphere packings with a resolution (voxel size) of 4% of nominal diameter a at best, while the diameter distribution extends at least to $\pm 0.03a$. In spite of serious efforts to eliminate the influence of size distribution by deconvoluting correlation data, their estimation of coordination numbers are well above the upper limit 6 in dense samples, which is in principle impossible. Practical measurements of coordination numbers would require an accuracy comparable to elastic deflections in the contact, *i.e.* $\kappa^{-1}a$, which is well beyond the reach of current experimental techniques for a bead packing. As to function $z(h)$, it is only safely evaluated in the experiments beyond the limit (approximately $0.04a$, see Fig. 9) where it ceases to be sensitive to the contact coordination number, and becomes chiefly dependent on solid fraction Φ. Such experiments are therefore unable to distinguish between samples A and C, despite their large difference in coordination number. We shall see (in paper III [38]) that measurements of elastic moduli are much better suited to obtain such information by experimental means.

V. CONCLUSIONS

The set of numerical results we have been presenting stresses the crucial importance of assembling processes of solidlike granular packings in the determination of their geometric and mechanical properties.

The frictionless case is an interesting limit, which coincides under isotropic pressure and in the rigid limit with the traditional notion of random close packing (RCP) state, provided the packing process is fast enough and minimizes traces of crystallization. This state appears then to be unique, independent on the way the rigid limit of a static packing is approached.

Our results (Section III) thus confirm the traditional view about RCP, which is supported by detailed numerical information. With friction, on the other hand (Sections IV A and IV B), there is a wide variety of possible states, even on maintaining fabric and stress isotropy, and without introducing cohesive forces. We found in particular that solid fraction Φ and coordination number z^* could vary independently in stable solid packings in mechanical equilibrium, and that rattler fractions above

10% could be observed. In particular, packings can be made with a density close to the RCP value and as few contacts as in the loosest configurations obtained by direct, slow isotropic compressions of granular gases.

Shapes of force distributions and mobilization of friction can also be affected by the compression step that follows the assembling stage in most mechanical characterization procedures. The correlations at short distances between neighbor positions depend on how rattlers are dealt with (Section IV C). Packings with lowest coordination numbers do not appear to lose force indeterminacy under small stresses, in spite of our low (comparatively to other numerical simulations) compression rates, at least for usual values of the coefficient of friction. The free mechanism motion asssociated with divalent grains does not jeopardize the stability of packings, and leads to a small correction on evaluating the degree of froce indeterminacy (hyperstaticity) h from the backbone coordination number z^*.

We sought experimental confrontations for our numerical results. Although the large scale features (say, beyond 5% of the diameter) of pair correlations and geometric structure can be compared to results of X-ray tomography (Section IV C and Appendix D), details of near neighbor correlations, or, worse, coordination numbers, are still not measurable in laboratory samples. But elastic moduli are, and enable confrontations between numerical and experimental data, as presented in paper III [38], in which elastic moduli are correlated to contact network microstructure. However, it is first necessary to assess the influence of the pressure level on the packing inner states. As hinted by the results of Table III, a quasistatic compression affects the force distribution and the level of friction mobilization. Elastic properties being usually measured above a certain confinement level (typically, a few tens of kPa), the necessary study of the effects of a quasistatic compression is carried out in paper II [37].

Other perspectives to the present work are the investigation of the microstructure of polydisperse packings, and of assemblies of non-spherical particles [103].

APPENDIX A: CONTACT ELASTICITY AND FRICTION

The contact law between spherical elastic bodies, with a Coulomb criterion for friction applied locally (to the surface force densities), leads to complicated history-dependent force-displacement relationships [39, 104]. Even in some cases with no slip anywhere in the contact region, the tangential stiffness K_T of a contact was shown [105] to depend on the past history of the contact loading, and to change according to the direction of the displacement increment. Strictly speaking, the response of intergranular contacts, even to arbitrary small load increments, should not be termed "elastic". The simplified law we adopted involves a tangential stiffness K_T depending on the normal deflection h, but independent of the current mobilization of friction (leading to slip in part of the contact surface [104]). This is the same approximation as used in [29, 30]: the value of K_T is the correct one in the absence of elastic relative tangential displacement, when $\mathbf{T} = 0$.

However, as stressed in [40], such a model is thermodynamically inconsistent, for the elastic energy might increase at no cost. Consider, *e.g.,* quasistatically reducing h at constant $\delta\mathbf{u}_T$, thereby, according to this contact model, reducing normal force N at constant $\mathbf{T}$, without reaching the Coulomb limit. The recoverable elastic energy stored in the contact is given by

$$w = \frac{2}{5}\tilde{E}\sqrt{a}h^{5/2} + \frac{1}{2}\frac{\mathbf{T}^2}{K_T}, \tag{A1}$$

which grows as K_T decreases, without the external force doing any work, thus implying a net creation of energy. To avoid such effects, $\mathbf{T}$ is rescaled (as advocated by O. Walton [106]), whenever N decreases to $N - \Delta N$, down to $\mathbf{T}\dfrac{K_T(N-\Delta N)}{K_T(N)}$, before accounting for tangential relative displacement increments. No such rule applies to increasing normal force cases. Such a procedure was shown by Elata and Berryman [40] to systematically produce energy dissipation in cyclic loadings of the contact.

Such peculiarities of the contact law affect the form and, in fact, the very definition of an elastic response of the contact network, an issue which will be discussed in paper III.

APPENDIX B: TRANSPORT OF CONTACT FORCES DUE TO PARTICLE MOTION

In molecular dynamics calculations, as well as in static approaches (as outlined in Section II C) one has to relate small contact force increments in any contact to the small displacements $\mathbf{u}_i$ and rotations $\Delta\theta_i$ of the grains.

Increments $\Delta(N_{ij}\mathbf{n_{ij}})$ and $\Delta\mathbf{T}_{ij}$ of the normal and tangential parts of the force in the contact between grains i and j have two different origins: they stem from the contact law, as written down in Section II, and they account for the motion of the particle pair. As the grains move, so does the deformed contact region, and therefore the resulting contact force. The relevant formulae are derived and written below for small increments in the static case. For dynamical computations, displacements are to be replaced by velocities, and increments by time derivatives.

The normal force variation is simply

$$\Delta(N_{ij}\mathbf{n}_{ij}) = \Delta N_{ij}\mathbf{n}_{ij} + N_{ij}\Delta\mathbf{n}_{ij}, \tag{B1}$$

with (for spheres of radii R_i, R_j)

$$\Delta\mathbf{n}_{ij} = \frac{1}{||\mathbf{r}_{ij}||}\left(\underline{\underline{\mathbf{1}}} - \mathbf{n}_{ij}\otimes\mathbf{n}_{ij}\right)\cdot\left(\tilde{\mathbf{u}}_j - \tilde{\mathbf{u}}_i - \underline{\underline{\epsilon}}\cdot\mathbf{r}_{ij}\right), \tag{B2}$$

while ΔN_{ij} is related by the Hertz law to the variation in the normal deflection of the contact (distance of the centers for spheres).

For the tangential reaction one may write

$$\Delta \mathbf{T}_{ij} = \Delta \mathbf{T}_{ij}^{(1)} + \Delta \mathbf{T}_{ij}^{(2)}$$

Increments with superscript (1) are associated, via the contact law, to the relative displacement of the contact point, which defines the constitutive part of the stiffness matrix discussed in Section II C.

Superscript (2) labels increments of kinematic origin. We assume that the magnitude of the contact force is unchanged in the absence of relative displacement at contact ($\delta \mathbf{u}_{ij} = 0$), and thus we write

$$\Delta \mathbf{T}_{ij}^{(2)} = \Delta \theta_{ij} \times \mathbf{T}_{ij}, \tag{B3}$$

with $\Delta\theta_{ij}$ the rotation of the contact region. $\Delta\theta_{ij}$ can be split in a *rolling* part $\Delta\theta_{ij}^{(R)}$, orthogonal to $\mathbf{n}_{ij}$, and a *pivoting* one, $\Delta\theta_{ij}^{(P)}$, along $\mathbf{n}_{ij}$. $\Delta\theta_{ij}^{(R)}$ is determined by the incremental change in $\mathbf{n}_{ij}$:

$$\Delta\theta_{ij}^{(R)} = \mathbf{n}_{ij} \times \Delta \mathbf{n}_{ij}. \tag{B4}$$

As to the pivoting part $\Delta\theta_{ij}^{(P)}$, it is natural to equate it to the average rotation of the two particles around the normal direction:

$$\Delta\theta_{ij}^{(P)} = \frac{1}{2}\mathbf{n}_{ij} \cdot (\Delta\theta_i + \Delta\theta_j)\, \mathbf{n}_{ij}. \tag{B5}$$

This choice is such that the rotation of the contact force coincides with the rotation of the pair in contact if both objects move together like one rigid body.

Injecting (B2) into Eqns. (B4) and (B5), one readily obtains the appropriate formula for $\Delta \mathbf{T}_{ij}^{(2)}$,

$$\begin{aligned}\Delta \mathbf{T}_{ij}^{(2)} =& -\left[\mathbf{T}_{ij} \cdot \left(\tilde{\mathbf{u}}_j - \tilde{\mathbf{u}}_i - \underline{\underline{\epsilon}} \cdot \mathbf{r}_{ij}\right)\right] \frac{\mathbf{n}_{ij}}{r_{ij}} \\ &+ \frac{1}{2}(\Delta\theta_i + \Delta\theta_j) \cdot (\mathbf{n}_{ij} \times \mathbf{T}_{ij}).\end{aligned}$$

With the notations of Section II C, the contribution of contact i, j to the 3×3 diagonal block of $\underline{\underline{\mathbf{K}}}^{(2)}$ which expresses the dependence of $\mathbf{F}_i^{\text{ext}}$ on displacement $\mathbf{u}_i$ is the non-symmetric tensor

$$-\frac{N_{ij}}{r_{ij}}(\underline{\underline{\mathbf{1}}} - \mathbf{n}_{ij} \otimes \mathbf{n}_{ij}) + \frac{\mathbf{n}_{ij} \otimes \mathbf{T}_{ij}}{r_{ij}}.$$

In general, the geometric stiffness matrix $\underline{\underline{\mathbf{K}}}^{(2)}$ is thus not symmetric, except in frictionless sphere packings, which are analogous to central force networks. In that case, $\underline{\underline{\mathbf{K}}}^{(2)}$ is a symmetric, negative matrix if forces are repulsive, as discussed by Alexander in his review on the elasticity of amorphous networks [87]. If the network has a mechanism in which two grains that are joined by a prestressed contact have a non-vanishing relative motion, then such a network cannot be stable. The potential energy of the externally applied load is strictly decreasing in that motion. This destabilizing effect can also be directly established in the rigid case, as shown in [32]. This is the reason why stable packings of frictionless spheres in equilibrium under some externally applied load are devoid of mechanisms (if only the force-carrying structure is considered).

In general stiffness matrices were discussed by Kuhn and Chang [50], and by Bagi [51]. Those authors gave general results for $\underline{\underline{\mathbf{K}}}^{(2)}$ with particles of arbitrary shapes, which coincide with ours in the case of spherical balls.

APPENDIX C: STRESS-CONTROLLED MOLECULAR DYNAMICS

It might be noted that the original Parrinello-Rahman equations slightly differ from ours. First, Eqn. (6) is written down with an additional term

$$m_i \ddot{s}_i^{(\alpha)} = \frac{1}{L_\alpha} F_i^{(\alpha)} - 2\frac{\dot{L}_\alpha}{L_\alpha} m_i \dot{s}_i^{(\alpha)}. \tag{C1}$$

Then, eqn. (7) is written with a different stress tensor, $\underline{\underline{\pi}}$, the definition of which involves a particular reference value $\underline{\underline{\mathbf{L_0}}}$ of the cell dimensions, for which the volume is Ω_0. $\underline{\underline{\pi}}$ is related to the Cauchy stress tensor $\underline{\underline{\mathbf{\Sigma}}}$ by

$$\underline{\underline{\pi}} = \frac{\Omega}{\Omega_0} \underline{\underline{\mathbf{L}}}_0 \cdot \underline{\underline{\mathbf{L}}}^{-1} \cdot \underline{\underline{\mathbf{\Sigma}}} \cdot {}^{\mathbf{T}}\underline{\underline{\mathbf{L}}}^{-1} \cdot {}^{\mathbf{T}}\underline{\underline{\mathbf{L}}}_0^{-1}. \tag{C2}$$

$\underline{\underline{\pi}}$ is a symmetric tensor known as the second Piola-Kirchhoff stress tensor [107] (also called *thermodynamic tension* by some authors, as in Refs. [108, 109], which might be consulted as they offer similar discussions of effects of preexisting stresses on the definitions of elastic moduli). Tensor $\underline{\underline{\pi}}$ can be used to express the power $\mathcal{P}/\Omega_0$ of internal forces, per unit volume in the reference (undeformed) configuration.

The *metric tensor* $\underline{\underline{\mathcal{G}}} = {}^{\mathbf{T}}\underline{\underline{\mathbf{L}}}_0^{-1} \cdot {}^{\mathbf{T}}\underline{\underline{\mathbf{L}}} \cdot \underline{\underline{\mathbf{L}}} \cdot \underline{\underline{\mathbf{L}}}_0^{-1}$ expresses the distance between current points as a function of their coordinates in the reference configuration. The difference between $\underline{\underline{\mathcal{G}}}$ and the unit tensor defines the Green-Lagrange strain tensor [107], $\underline{\underline{\mathbf{e}}}$, as

$$\underline{\underline{\mathbf{e}}} = -\frac{1}{2}\left(\underline{\underline{\mathcal{G}}} - \underline{\underline{\mathbf{I}}}\right). \tag{C3}$$

Then $\underline{\underline{\pi}}$ is such that, for whatever strain history

$$\mathcal{P} = \Omega_0 \underline{\underline{\pi}} : \dot{\underline{\underline{\mathbf{e}}}}. \tag{C4}$$

If the last term of Eqn. (7) is replaced by $\dfrac{(L_0^\alpha)^2}{\Omega_0 L_\alpha}$, and if (C1) is used instead of (6), then, in the case when interparticle forces derive from a potential V, function of particle positions $\mathbf{r}_i$ and orientations, the system of

equations conserves the total energy

$$H = \frac{1}{2}\sum_i m_i \dot{\mathbf{s}}_i \cdot {}^{\mathrm{T}}\underline{\underline{\mathbf{L}}} \cdot \underline{\underline{\mathbf{L}}} \cdot \dot{\mathbf{s}}_i + \frac{1}{2}\sum_i I_i \omega_i^2 + V + \frac{1}{2} M \cdot {}^{\mathrm{T}}\underline{\underline{\dot{\mathbf{L}}}} : \underline{\underline{\dot{\mathbf{L}}}} + V + \frac{\Omega_0}{2}\underline{\underline{\mathcal{G}}} : \underline{\underline{\pi}}. \quad \text{(C5)}$$

Such equations would tend to impose a constant Piola-Kirchhoff stress.

Granular assemblies are however dissipative systems, and energy conservation is not a crucial issue as in molecular systems. In practice, we observed that omission of the extra term of (C1) as well as control of Cauchy, rather than Piola-Kirchhoff stresses, did not affect the approach to equilibrium configurations. On considering small motions and elastic properties close to an equilibrium configuration, as in Section II C, one may prefer dealing with external forces deriving from a potential. We note that this is indeed the case if we use Eqns. (C1) and (7) with an isotropic $\underline{\underline{\mathbf{\Sigma}}}$, $\underline{\underline{\mathbf{\Sigma}}} = P\underline{\underline{\mathbf{1}}}$, in which case the external stress control is associated with potential energy $P\Omega$ (instead of the last term in Eqn. C5).

APPENDIX D: COMPARISON OF LOCAL BOND ORDER PARAMETERS WITH EXPERIMENTAL OBSERVATIONS

Although the samples were not isotropic, owing to the role of gravity in the preparation stage, and not perfectly homogeneous, because of lateral walls, the experiments performed by Aste *et al.* [7] provided an unprecedented wealth of results on the geometry of sphere packings. The local arrangement of neighbors around one bead were classified according to the values taken by the pair $(Q_4^{\mathrm{loc}}(i), Q_6^{\mathrm{loc}}(i)$, for different choices of the distance d_c that defines the bonds. For each sample and choice of d_c, the proportion of spheres having the most frequent range of values $(\hat{Q}_4 \pm 0.05, \hat{Q}_6 \pm 0.05)$ corresponding to some typical disordered arrangement was recorded, as well as the frequency of occurrence of values $(0.191 \pm 0.05, 0.574 \pm 0.05)$ and $(0.097 \pm 0.05, 0.485 \pm 0.05)$ respectively corresponding to fcc-like and hcp-like local ordering. Those values are compared to the ones we observed in numerical samples of similar density in tables VII and VIII (we kept the same $(\hat{Q}_4, \hat{Q}_6)$ couple). The fraction of beads with the typical disordered configuration of neighbors (marked *dis.* in the tables) are very close in numerical packings and in the experimental one of the same densities, and the frequency of occurrence of hcp-like local environments also compares well, although it does not seem to share the same dependence on the threshold distance d_c defining bonds. However, the small fraction of fcc-like beads observed in the laboratory is absent in the simulations. Many cirmcumstances can be invoked to explain these differences, including of course the different packing history of the numerical and experimental samples, which in the the latter case involves gravity and anisotropy. It can be remarked once again that A' samples are a little more ordered than A ones (with slightly larger fractions of hcp-like local configurations), from which C samples are quite indistinguish-

TABLE VII: Most frequently values $(\hat{Q}_4(i), \hat{Q}_6(i))$ observed in the measurements of [7] in a dense sample ($\Phi = 0.640 \pm 0.005$, called sample F in [7]), and fraction (*dis.*) of local configurations within interval $(\hat{Q}_4 \pm 0.05, \hat{Q}_6 \pm 0.05)$ obtained in experiments and in numerical simulations with similar densities : A, A' and C.

Sample	d_c	$(\hat{Q}_4, \hat{Q}_6)$	*dis* (%)	*fcc* (%)	*hcp* (%)
Aste *et al.*	1.1	(0.23, 0.44)	31	6	4
dense	1.2	(016, 0.45)	38	4	12
$\Phi \simeq 0.640$	1.3	(0.13, 0.42)	43	1	17
(F in [7])	1.4	(0.10, 0.38)	47	3	13
A	1.1	(same	32	$< 10^{-2}$	4
A	1.2	values	37	$< 10^{-2}$	5
A	1.3	as	43	$< 10^{-2}$	8
A	1.4	above)	46	$< 10^{-2}$	12
A'	1.1	(same	31	$< 10^{-2}$	5
A'	1.2	values	40	$< 10^{-2}$	6
A'	1.3	as	45	$< 10^{-2}$	10
A'	1.4	above)	48	$< 10^{-2}$	15
C	1.1	(same	31	$< 10^{-2}$	4
C	1.2	values	37	$< 10^{-2}$	5
C	1.3	as	43	$< 10^{-2}$	8
C	1.4	above)	46	$< 10^{-2}$	13

TABLE VIII: Same as table VII for experimental samples of lower densities, one with $\Phi = 0.626 \pm 0.008$ (called sample D in [7]), another with $\Phi = 0.596 \pm 0.006$ (called sample B in [7]), to which values obtained in simulated samples B and D, of similar densities, are respectively compared.

Sample	d_c	$(\hat{Q}_4, \hat{Q}_6)$	*dis* (%)	*fcc* (%)	*hcp* (%)
Aste *et al.*	1.1	(0.25, 0.44)	28	4	1
	1.2	(0.19, 0.44)	35	2	7
$\Phi \simeq 0.626$	1.3	(0.15, 0.40)	42	1	11
(D in [7])	1.4	(0.11, 0.36)	46	1	8
B	1.1	(same	30	$< 10^{-2}$	2.7
B	1.2	values	38	$< 10^{-2}$	7.6
B	1.3	as	43	$< 10^{-2}$	10
B	1.4	above)	46	$< 10^{-2}$	10
Aste *et al.*	1.1	(0.30, 0.45)	24	3	1
loose	1.2	(0.23, 0.44)	32	2	3
$\Phi \simeq 0.596$	1.3	(0.16, 0.38)	37	1	5
(B in [7])	1.4	(0.14, 0.35)	43	2	5
D	1.1	(same	24	$< 10^{-2}$	1.0
D	1.2	values	32	$< 10^{-2}$	4.4
D	1.3	as	37	$< 10^{-2}$	6.1
D	1.4	above)	43	$< 10^{-2}$	7.5

able, as the quantities measured here do not depend on whether pairs of neighbors are actually in contact.

APPENDIX E: ANALYSIS OF THE FREE MOTION OF DIVALENT SPHERES

We first give here the appropriate formulae to describe the free motion of divalent grains, then report on numerical stability tests.

The equations are specialized to the case of equal-sized spheres of dimater a, as in all the simulations reported in the present paper. Let i denote the label of the divalent grain in contact with its neighbors labelled j and k. The line joining the centers of j and k is parallel to unit vector $\mathbf{e}$, defined as

$$\mathbf{e} = \frac{\mathbf{n}_{ik} - \mathbf{n}_{ij}}{||\mathbf{n}_{ik} - \mathbf{n}_{ij}||},$$

and the distance D of the center of i to this line is

$$D = a\sqrt{1 - (\mathbf{e} \cdot \mathbf{n}_{ij})^2}.$$

ω_0 denoting the angular velocity of the center of i about this axis, the translational velocity of i, in its free motion depicted on Fig. 14, will be

$$\mathbf{v}_i = \omega_0 D \mathbf{t}, \tag{E1}$$

the unit vector $\mathbf{t}$ being orthogonal to the plane containing the centers of i, j, and k:

$$\mathbf{t} = \frac{\mathbf{n}_{ij} \times \mathbf{n}_{ik}}{||\mathbf{n}_{ik} \times \mathbf{n}_{ij}||}.$$

Its angular velocity will be

$$\mathbf{\Omega}_i = 2\omega_0 \mathbf{e}. \tag{E2}$$

With such a choice, the instantaneous velocity of the contact points between i and j, or between i and k satisfy:

$$\mathbf{v}_i + \mathbf{\Omega}_i \times \frac{a}{2}\mathbf{n}_{ij} = \mathbf{v}_i + \mathbf{\Omega}_i \times \frac{a}{2}\mathbf{n}_{ik} = 0,$$

as requested in a relative motion which is a combination of rolling and pivoting.

Let us now check that the rules defined in Appendix B ensure that the tangential components of the contacts i, j and i, k rotate with the contact points around the axis joining the centers of k and j with angular velocity ω_0. To describe this motion, let us define $\mathbf{f} = \mathbf{e} \times \mathbf{t}$. Vectors $\mathbf{f}$ and $\mathbf{t}$ rotate in the plane orthogonal to $\mathbf{e}$, with angular velocity ω_0, whence

$$\frac{d\mathbf{f}}{dt} = \omega_0 \mathbf{t} \quad \text{and} \quad \frac{d\mathbf{t}}{dt} = -\omega_0 \mathbf{f},$$

and $\mathbf{n}_{ij}$, as a function of time, satisfies

$$\mathbf{n}_{ij}(t) = \mathbf{e}\cos\alpha - \mathbf{f}(t)\sin\alpha, \tag{E3}$$

α being the angle between $\mathbf{e}$ and $\mathbf{n}_{ij}$. Starting at $t = 0$ with $\mathbf{T}_{ij} = T(\mathbf{e}\sin\alpha + \mathbf{f}\cos\alpha)$, which is the equilibrium form of the tangential force in contact i, j, $\mathbf{T}_{ij}$ satisfies, from Eqns. B3, B4 and B5,

$$\frac{d\mathbf{T}_{ij}}{dt} = -\frac{d\mathbf{n}_{ij}}{dt} \cdot \mathbf{T}_{ij} + \frac{1}{2}(\mathbf{n}_{ij} \cdot \mathbf{\Omega}_i)\mathbf{n}_{ij} \times \mathbf{T}_{ij}. \tag{E4}$$

The first term of (E4) vanishes if both $\mathbf{n}_{ij}$ and $\mathbf{T}_{ij}$ are in the $\mathbf{e}$, $\mathbf{f}$ plane, under which condition the second one yields, exploiting (E2)

$$\frac{d\mathbf{T}_{ij}}{dt} = \omega_0(\mathbf{n}_{ij} \cdot \mathbf{e})\mathbf{n}_{ij} \times \mathbf{T}_{ij} = \omega_0 \mathbf{e} \times \mathbf{T}_{ij}. \tag{E5}$$

Thus $\mathbf{T}_{ij}$ exactly follows the rotation of bead i around the j-k axis, and the solution to (E4) is

$$\mathbf{T}_{ij}(t) = T_{ij}(\mathbf{e}\sin\alpha + \mathbf{f}(t)\cos\alpha)$$

as announced. In other words, the geometric stiffness matrix $\underline{\underline{\mathbf{K}}}^{(2)}$ does not determine whether the mechanism associated with a two-coordinated bead is stable.

We checked for stability with numerical means, as follows. Starting from an equilibrium configuration, we first choose the potentially dangerous mechanisms, those involving relatively large contact forces, of the order of the average normal force or even larger. Thus, grains j and k undergo significant changes in the moment of the contact force with the mobile grain i. Then one such mobile divalent bead is attributed a velocity and a angular velocity according to Eqns. E1 and E2, with a value of ω_0 small enough for the centrifugal acceleration to be negligible (equal to $10^{-4}||\mathbf{F}_{ij}||$). The evolution of the whole grain packing under constant stress is then simulated with MD. Such numerical experiments were performed with the most fragile packings, D samples under low confining pressures. In all cases studied, as expected, the motion of the mechanism entails very slow changes in the configuration, if any. The mobile grain maintains a constant angular velocity while nearly exactly following its circular trajectory for a long time, with hardly any change in kinetic energy. These calculations in fact request more time steps than a compression step of the whole packing in which P increases by $\sqrt{10}$, and we therefore limited our investigations to 10 tests for 2 pressure levels in the D series, $P = 1$ kPa and $P = 10$ kPa. At the lowest pressure $P = 1$ kPa, corresponding to $\kappa \simeq 181000$, these motions were often observed to lead to a small rearrangement of the packing, in which kinetic energy spreads over all degrees of freedom, a significant fraction of the contacts, up to 25%, go through a sliding stage, the contact network is slightly modified and the system restabilizes in a slightly different configuration, with a small density increase (typically of order 10^{-5}). In other cases, the freely moving grain stops when it collides with a third grain other than the two with which it is maintaining contact. The system then finds a new equilibrium configuration without rearranging, only a few contacts temporarily reach a sliding

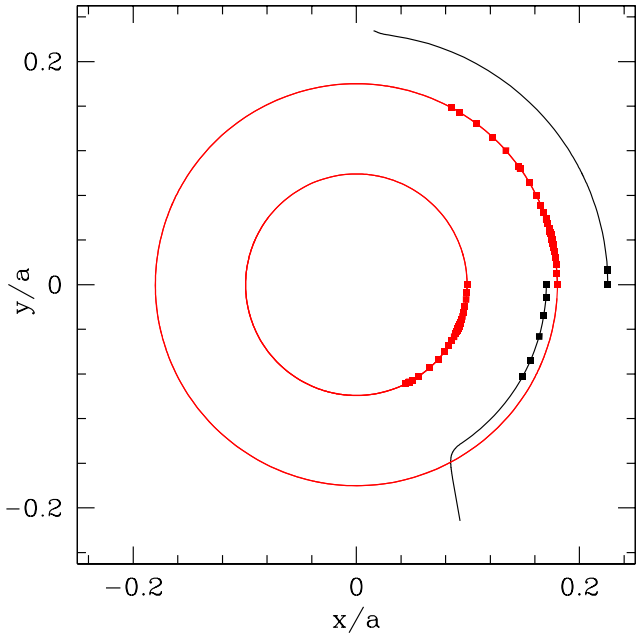

FIG. 16: (Color online) Examples of trajectories of mobile divalent grains in **f**, **t** plane. All trajectories begin at $x = D$, $y = 0$. Continuous lines depict the results obtained on ignoring contact creation, which end up, in 2 cases out of the 4 represented, in instabilities (black lines), while complete circles are observed in the other, stable ones (red). Dots mark the same trajectories, which are in practice arrested by other contacts when contact creation is taken into account.

status. On repeating similar tests at a larger confining pressure, $P = 10$ kPa (still close to the rigid limit), the occurrence of this second scenario became much more frequent than the first, which was never observed in the 10 tests performed.

The difference between stable and unstable cases is better appreciated on redoing the tests with a modified MD calculation method, in which only the initially existing contacts are taken into account. Thus one only investigates the properties of the pre-existing contact network. If it breaks, the system globally falls apart, and nearly all contacts in the packing eventually open. This is the unstable case. In the stable case, on the other hand, the mobile particle can turn several times around the line of centers of its two contacting neighbors without notable changes in kinetic energy and the contact network is maintained. This behavior is illustrated on Fig. 16, which displays trajectories of mobile grains in the plane orthogonal to **e**. Note that such a procedure reveal instabilities that are prevented by the appearance of a third contact of the mobile grain, and hence overestimates the frequency of occurrence of unstable configurations. 8 out of 10 such tests led to an instability in D samples under 1 kPa. This proportion fell to 2 out of 10 under 10 kPa.

Two possible conclusions may be drawn. On the one hand we may deem the D configurations under low pressures imperfectly stabilized, as some free motions might eventually cause configurational changes. Or, since anyway the evolution is so slow, it may be pointed out, on the other hand, that the slightest amount of dissipation in rolling would stop the free motion. In realistic systems the velocity a a free rolling motion always decays in time. Also, a very small amount of global damping would stop the motion. "Global damping" means that viscous forces are applied to the grains while they move relatively to a fixed reference frame, as through a viscous fluid saturating the intergranular voids in a fixed container.

Since the obtention of stable, equilibrated states in which all divalent grains have been made 3-coordinated would be very computationnally very costly, and as the occurrence of small instabilities related to such mechanisms appear to decrease fastly under growing confinement, we adopted the second attitude and regarded D and C configurations with a few percent of divalent particles as acceptable equilibrium states.

[1] H. J. Herrmann, J.-P. Hovi, and S. Luding, eds., *Physics of Dry Granular Media* (Balkema, Dordrecht, 1998).

[2] H. Hinrichsen and D. E. Wolf, eds., *The Physics of Granular Media* (Wiley-VCH, Berlin, 2004).

[3] R. García Rojo, H. J. Herrmann, and S. McNamara, eds., *Powders and Grains 2005* (Balkema, Leiden, 2005).

[4] A. J. Liu and S. R. Nagel, eds., *Jamming and rheology* (Taylor & Francis, New York, 2001).

[5] P. Richard, P. Philippe, F. Barbe, S. Bourlès, X. Thibault, and D. Bideau, PRE **68**, 020301(R) (2003).

[6] T. Aste, M. Saadatfar, A. Sakellariou, and T. J. Senden, Physica A **339**, 16 (2004).

[7] T. Aste, M. Saadatfar, and T. J. Senden, PRE **71**, 061302 (2005).

[8] D. Cumberland and R. Crawford, *The Packing of Particles* (Elsevier, Amsterdam, 1987).

[9] D. Bideau and J. Dodds, eds., *Physics of Granular Media* (Nova Science Publishers, 1991).

[10] S. Torquato, T. M. Truskett, and P. G. Debenedetti, Physical Review Letters **84**, 2064 (2000).

[11] D. M. Wood, *Soil Behaviour and Critical State Soil Mechanics* (Cambridge University Press, 1990).

[12] J. Biarez and P.-Y. Hicher, *Elementary Mechanics of Soil Behaviour* (A. A. Balkema, Rotterdam, 1993).

[13] J. K. Mitchell, *Fundamentals of soil behavior* (Wiley, New York, 1993).

[14] M. Oda, Soils and Foundations **12**, 17 (1972).

[15] J. R. F. Arthur and B. K. Menzies, Géotechnique **22**, 115 (1972).

[16] S. Fukushima and F. Tatsuoka, Soils and Foundations **24**, 40 (1984).

[17] L. Vanel, D. Howell, D. Clark, R. P. Behringer, and E. Clément, Phys. Rev. E **60**, R5040 (1999).

[18] P. A. Cundall and O. D. L. Strack, Géotechnique **29**, 47 (1979).
[19] R. J. Bathurst and L. Rothenburg, Mechanics of Materials **9**, 65 (1990).
[20] F. Radjai and S. Roux, in [110], pp. 21–24.
[21] F. Radjai and S. Roux, in [2], pp. 165–187.
[22] L. Rothenburg and N. P. Kruyt, International Journal of Solids and Structures **41**, 5763 (2004).
[23] J.-N. Roux and F. Chevoir, Bulletin des Laboratoires des Ponts et Chaussées **254**, 109 (2005).
[24] L. E. Silbert, D. Ertaş, G. S. Grest, T. C. Halsey, and D. Levine, Physical Review E **65**, 031304 (2002).
[25] L. E. Silbert, G. S. Grest, and J. W. Landry, Physical Review E **66**, 061303 (2002).
[26] H. Makse, D. Johnson, and L. Schwartz, Physical Review Letters **84**, 4160 (2000).
[27] C. Thornton, Géotechnique **50**, 43 (2000).
[28] A. S. J. Suiker and N. A. Fleck, ASME Journal of Applied Mechanics **71**, 350 (2004).
[29] H. Makse, N. Gland, D. Johnson, and L. Schwartz, Physical Review Letters **83**, 5070 (1999).
[30] H. A. Makse, N. Gland, D. L. Johnson, and L. Schwartz, Physical Review E **70**, 061302 (2004).
[31] C. O'Hern, L. E. Silbert, A. J. Liu, and S. R. Nagel, Physical Review E **68**, 011306 (2003).
[32] J.-N. Roux, Physical Review E **61**, 6802 (2000).
[33] N. S. Rad and M. T. Tumay, ASTM Journal of Geotechnical Testing **10**, 31 (1987).
[34] N. Benahmed, J. Canou, and J.-C. Dupla, Comptes-Rendus Académie des Sciences, Mécanique **332**, 887 (2004).
[35] E. R. Nowak, J. B. Knight, E. Ben-Naim, H. M. Jaeger, and S. R. Nagel, Physical Review E **57**, 1971 (1998).
[36] P. Philippe and D. Bideau, Europhysics Letters **60**, 677 (2002).
[37] I. Agnolin and J.-N. Roux, *Internal states of model isotropic granular packings: compression and pressure cycles*, first companion paper, second in the series (2007).
[38] I. Agnolin and J.-N. Roux, *Internal states of model isotropic granular packings: elastic properties*, second companion paper, third in the series (2007).
[39] K. L. Johnson, *Contact Mechanics* (Cambridge University Press, 1985).
[40] D. Elata and J. G. Berryman, Mechanics of Materials **24**, 229 (1996).
[41] M. Parrinello and A. Rahman, Journal of Applied Physics **52**, 7182 (1981).
[42] J. Christoffersen, M. M. Mehrabadi, and S. Nemat-Nasser, Journal of Applied Mechanics **48**, 339 (1981).
[43] J.-P. Hansen and I. R. McDonald, *Theory of Simple Liquids* (Academic Press, 1986).
[44] P. Cundall, in *Micromechanics of Granular Materials*, edited by M. Satake and J. T. Jenkins (Elsevier, Amsterdam, 1988), pp. 113–123.
[45] F. A. Gilabert, J.-N. Roux, and A. Castellanos, Phys. Rev. E **75**, 011303 (2007).
[46] B. Servatius and H. Servatius, in [52], pp. 1–19.
[47] S. McNamara, R. García Rojo, and H. J. Herrmann, Physical Review E **72**, 021304 (2005).
[48] S. McNamara and H. J. Herrmann, Physical Review E **74**, 061303 (2006).
[49] E. Somfai, J.-N. Roux, J. Snoeijer, M. van Hecke, and W. van Saarloos, PRE **72**, 021301 (2005).
[50] M. R. Kuhn and C. S. Chang, International Journal of Solids and Structures **43**, 6026 (2006).
[51] K. Bagi, Granular Matter **9**, 109 (2007).
[52] M. F. Thorpe and P. M. Duxbury, eds., *Rigidity Theory and Applications*, Fundamental Materials Research (Kluwer Academic, 1998).
[53] A. Donev, S. Torquato, and F. H. Stillinger, PRE **71**, 011105 (2005).
[54] G. Combe and J.-N. Roux, in *Deformation characteristics of geomaterials*, edited by H. di Benedetto, T. Doanh, H. Geoffroy, and C. Sauzéat (Swets and Zeitlinger, Lisse, 2003), pp. 1071–1078.
[55] F. Tatsuoka, M. Sakamoto, T. Kawamura, and S. Fukushima, Soils and Foundations **26**, 65 (1986).
[56] G. Reydellet and E. Clément, Physical Review Letters **86**, 3308 (2001).
[57] G. Combe, *Mécanique des matériaux graulaires et origines microscopiques de la déformation* (Presses du Laboratoire Central des Ponts et Chaussées, Paris, 2002).
[58] G. MIDI, European Physical Journal E **14**, 341 (2004).
[59] F. da Cruz, S. Emam, M. Prochnow, J.-N. Roux, and F. Chevoir, Physical Review E **72**, 021309 (2005).
[60] O. Pouliquen, C. Cassar, Y. Forterre, P. Jop, and M. Nicolas, in [3], pp. 859–865.
[61] P. Jop, Y. Forterre, and O. Pouliquen, Journal of Fluid Mechanics **541**, 167 (2005).
[62] P. Jop, Y. Forterre, and O. Pouliquen, Nature **44**, 727 (2006).
[63] B. J. Alder and T. E. Wainwright, J. Chem. Phys. **31**, 459 (1959).
[64] B. D. Lubachevsky and F. H. Stillinger, Journal of Statistical Physics **60**, 561 (1990).
[65] B. D. Lubachevsky, F. H. Stillinger, and E. N. Pinson, Journal of Statistical Physics **64**, 501 (1991).
[66] A. Donev, S. Torquato, F. H. Stillinger, and R. Connelly, Journal of Computational Physics **197**, 139 (2004).
[67] I. Volkov, M. Cieplak, J. Koplik, and J. R. Banavar, Physical Review E **66**, 061401 (2002).
[68] R. Connelly, Structural Topology **14**, 43 (1988).
[69] A. R. Kansal, S. Torquato, and F. H. Stillinger, Physical Review E **66**, 041109 (2002).
[70] V. Luchnikov, A. Gervois, P. Richard, L. Oger, and J.-P. Troadec, Journal of Molecular Liquids **96-97**, 185 (2002).
[71] S. Emam, J.-N. Roux, J. Canou, A. Corfdir, and J.-C. Dupla, in [3], pp. 49–52.
[72] N. Benahmed, Ph.D. thesis, École Nationale des Ponts et Chaussées, Champs-sur-Marne, France (2001).
[73] S. Ouaguenouni and J.-N. Roux, Europhysics Letters, **39**, 117 (1997).
[74] J.-N. Roux, in *Proceedings of the Saint-Venant Symposium on Multiple Scale Analysis and Coupled Physical Systems* (Presses de l'Ecole Nationale des Ponts et Chaussées, Paris, 1997), pp. 577–584.
[75] C. F. Moukarzel, Physical Review Letters **81**, 1634 (1998).
[76] C. F. Moukarzel, in [52], pp. 125–142.
[77] A. Tkachenko and T. A. Witten, Physical Review E **60**, 627 (1999).
[78] C. F. Moukarzel, Granular Matter **3**, 41 (2001).
[79] C. F. Moukarzel, in [2], pp. 23–43.
[80] A. Donev, S. Torquato, F. H. Stillinger, and R. Con-

nelly, PRE **70**, 043301 (2004).
[81] C. O'Hern, L. E. Silbert, A. J. Liu, and S. R. Nagel, Physical Review E **70**, 043302 (2004).
[82] G. Y. Onoda and E. G. Liniger, Physical Review Letters **64**, 2727 (1990).
[83] *Détermination des masses volumiques minimales et maximales des sols non cohérents*, French Standard NFP 94-059 (1992).
[84] M. M. Kohonen, D. Geromichalos, M. Scheel, C. Schier, and S. Herminghaus, Physica A **39**, 7 (2004).
[85] F. de Larrard, *Concrete mixture proportioning, a scientific approach* (Routledge, London, 1999).
[86] X. Jia and P. Mills, in [110], pp. 105–112.
[87] S. Alexander, Phys. Rep. **296**, 65 (1998).
[88] S. Ouaguenouni and J.-N. Roux, in [111], pp. 188–191.
[89] M. E. Cates, J. P. Wittmer, J.-P. Bouchaud, and P. Claudin, Physical Review Letters **81**, 1841 (1998).
[90] F. Radjai, M. Jean, J.-J. Moreau, and S. Roux, Phys. Rev. Lett. **27**, 274 (1996).
[91] S. J. Antony, Phys. Rev. E **63**, 011302 (2000).
[92] D. M. Mueth, H. M. Jaeger, and S. R. Nagel, Phys. Rev. E **57**, 3164 (1998).
[93] D. L. Blair, N. W. Mueggenburg, A. H. Marshall, H. Jaeger, and S. R. Nagel, Physical Review E **63**, 041304 (2001).
[94] F. Radjai, D. Wolf, S. Roux, M. Jean, and J.-J. Moreau, in [111], pp. 169–179.
[95] F. Radjai, D. E. Wolf, M. Jean, and J.-J. Moreau, Physical Review Letters **80**, 61 (1998).
[96] H. P. Zhang and H. A. Makse, Physical Review E **72**, 011301 (2005).
[97] G. T. Nolan and P. E. Kavanagh, Powder Technology **72**, 149 (1992).
[98] W. M. Visscher and M. Bolsterli, Nature **239**, 504 (1972).
[99] R. Jullien and P. Meakin, Europhysics Letters **4(12)**, 1385 (1987).
[100] G. C. Barker and A. Mehta, Physical Review A **45**, 3435 (1992).
[101] A. Mehta, G. C. Barker, and J. M. Luck, Journal of Statistical Mechanics: Theory and Experiment p. P10014 (2004).
[102] I. Bratberg, F. Radjai, and A. Hansen, Physical Review E **66**, 031303 (2002).
[103] A. Donev, R. Connelly, F. H. Stillinger, and S. Torquato, *Hypostatic Jammed Packings of Nonspherical Hard Particles: Ellipses and Ellipsoids*, preprint (archive cond-mat 0608334) (2006).
[104] R. D. Mindlin and H. Deresiewicz, ASME Journal of Applied Mechanics **20**, 327 (1953).
[105] D. L. Johnson and A. N. Norris, Journal of Mechanics and Physics of Solids **45**, 1025 (1997).
[106] O. Walton, *private communication.*
[107] J. Salençon, *Handbook of continuum mechanics. General concepts, Thermoelasticity.* (Springer, 2001).
[108] J. R. Ray and A. Rahman, JCP **76**, 4423 (1984).
[109] A. Lemaître and C. Maloney, Journal of Statistical Physics **123**, 415 (2006).
[110] Y. Kishino, ed., *Powders and Grains 2001* (Swets & Zeitlinger, Lisse, 2001).
[111] D. Wolf and P. Grassberger, eds., *Friction, Arching, Contact Dynamics* (World Scientific, Singapore, 1997).